Journal of Hyperbolic Differential Equations
Vol. 11, No. 2 (2014) 295–328

DOI: 10.1142/S021989161450009X

World Scientific
www.worldscientific.com

Combustion waves and Riemann solutions in light porous foam

G. Chapiro*
Department of Geoscience & Engineering
Delft University of Technology, Stevinweg 1
Delft 2628CN, The Netherlands
grigori@ice.ufjf.br

D. Marchesin
Instituto Nacional de Matemática Pura e Aplicada
Estrada Dona Castorina 110, Rio de Janeiro
RJ 22460-320, Brazil
marchesi@impa.br

S. Schecter
Mathematics Department
North Carolina State University
Raleigh, NC 27695-8205, USA
schecter@math.ncsu.edu

Received 4 June 2013
Accepted 31 March 2014
Published 30 May 2014

Communicated by P. Marcati

Abstract. We prove the existence of traveling waves, and identify the wave sequences appearing in Riemann solutions, for a system of three evolutionary partial differential equations that models combustion of light porous foam under air injection.

Keywords: Traveling wave; Riemann problem; filtration combustion; combustion in porous media; ignition; extinction.

Mathematics Subject Classification 2010: 35L67, 35C07, 35K57, 34C37, 80A25, 76S05

1. Introduction

This paper is part of long-term research project to identify waves that arise in one-dimensional models of flow in porous media, especially models relevant to various methods of oil recovery, and to understand how the waves fit together in solutions of boundary value problems (BVPs); see [4–6, 11–14, 17] and references therein. Flows

*On leave from Departamento de Matemática, Universidade Federal de Juiz de Fora, Juiz de Fora, MG 36036-900, Brazil.

that involve combustion give rise to reaction–convection–diffusion equations in which the three aspects are of roughly equal importance. None can be safely ignored.

The paper is motivated by a model for the injection of air into a porous medium that contains a solid fuel. The model was proposed in [1] and further studied in [5, 6]. We simplify the model by ignoring the dependence of gas density on temperature. Our study was motivated by a desire to find a model that (1) reproduces the variety of phenomena observed when air is injected into a porous medium containing a solid fuel, yet (2) is simple enough to permit a rigorous investigation. Our simplification allows proofs of existence of traveling waves by phase plane analysis. We also identify the wave sequences that can occur as solutions of Riemann problems.

Our model, which is described in Sec. 2 and derived in Appendix A, consists of three equations that express energy, oxygen, and fuel balance laws. We use a shifted Arrhenius law for which combustion begins at a threshold temperature. We analyze the case in which the thermal capacity of the medium is negligible compared to that of air. A consequence is that oxygen and heat are both transported at the velocity of the moving gas. The thermal capacity assumption is not correct for oil recovery, but is approximately valid for polyurethane foam such as that used in furniture.

We find four types of combustion waves that approach their end states exponentially, two that propagate faster than oxygen and temperature, and two that propagate more slowly. Fast combustion waves represent "premixed combustion": combustion, once it starts, races, in the form of a burning front, into a region where both solid fuel and oxygen are present. Behind the front either oxygen or fuel is exhausted. The slow combustion waves we find have been called "reaction-trailing smolder waves" [18] and "coflow (or forward) filtration combustion waves" [2] in the context of more complicated models of injection of air into a porous medium. The moving gas brings oxygen into a region where solid fuel is present. The oxygen is consumed in the reaction. Since the gas velocity is greater than that of the flame front, a region of high temperature and no oxygen is swept ahead of the front. Both fast and slow combustion waves are described in Sec. 3.

"Reaction-leading smolder waves", observed in both [18, 2], are not seen in our model. These are slow combustion waves in which the high-temperature region lies behind the wave. We expect to see these waves if we assume that oxygen is transported faster than heat. This will be the subject of future research.

For initial-BVPs on an infinite interval with constant boundary data, one expects the solution to resolve into combustion waves and intervals in which combustion does not occur. On these intervals the equations decouple, so one expects to observe standing solid fuel concentration patterns, convected oxygen concentration patterns, and temperature waves. Viewed from a distance, these waves resemble contact discontinuities. In Sec. 4, we show that only certain contact discontinuities can occur in generic wave sequences.

In Sec. 5, we present the generic wave sequences that could be observed for large time. For some boundary conditions, several different wave sequences are possible; they are expected to be observed for different initial data. The most complicated

of the wave sequences include both a slow and a fast combustion wave. We present numerical simulations in which the expected wave sequences occur.

Since we only consider generic boundary data, we do not consider the possibility that at one end, combustion fails to occur for more than one reason. For example, we do not consider the possibility that at the right, there is both no oxygen and a low temperature. Some such BVPs are of course physically important, and will be the subject of future research.

Our system can be rewritten as one balance law coupled to two conservation laws, which allow reduction of the traveling wave system to two dimensions. In Sec. 6, we perform this reduction and study equilibria of the traveling wave system. In Secs. 7 and 8, existence of the various combustion waves is proved.

Let us comment briefly on our use of a shifted Arrhenius factor, so that combustion begins at a threshold temperature above absolute zero, and the combustion rate depends continuously on temperature. In analytical studies of combustion waves in porous media, such as [1–4, 11, 18, 19], it is more typical to replace the Arrhenius factor by zero below a fixed fraction of combustion temperature [20], resulting in discontinuous dependence of the reaction rate on temperature. We do not think this would change the results, but it would complicate the presentation. We believe that our choice is appropriate when analyzing simplified equations.

The cited papers assume the existence of various combustion waves and investigate their properties using asymptotic expansion. Recent papers that used a shifted Arrhenius factor and use nonperturbative methods to prove the existence of combustion waves in simplified models include [7], which uses the method of upper and lower solutions, and [13, 14, 17], which use Geometric Singular Perturbation Theory [10].

In our simplified model, it should be possible to rigorously investigate the time-asymptotic stability of the combustion waves. The papers [9, 8] propose an approach to stability analysis of combustion waves that we expect to prove useful for this.

2. Model

The system we consider is

$$\partial_t \theta + a\partial_x \theta = \partial_{xx}\theta + \rho Y \Phi, \tag{2.1}$$

$$\partial_t \rho = -\rho Y \Phi, \tag{2.2}$$

$$\partial_t Y + a\partial_x Y = -\rho Y \Phi, \tag{2.3}$$

$$\Phi = \begin{cases} \exp(-1/\theta), & \theta > 0, \\ 0, & \theta \le 0. \end{cases} \tag{2.4}$$

There are three dependent dimensionless variables: temperature θ, solid fuel concentration ρ, and oxygen concentration Y. The oxygen is a component of a gas that is moving with velocity $a > 0$. Both oxygen and heat are assumed to be transported with this velocity. An exothermic chemical reaction involving oxygen and the solid

fuel can occur only when the temperature is above a threshold temperature, which we normalize to be $\theta = 0$. Because of this convention, the temperature is allowed to be negative. The unit reaction rate is given in (2.4) by $\Phi(\theta)$. Equation (2.1) represents transport and diffusion of temperature, and generation of thermal energy by the chemical reaction. Equation (2.2) represents consumption of the solid fuel, which of course does not diffuse and is not transported by the gas. Equation (2.3) represents transport of oxygen and consumption of oxygen in the chemical reaction. Diffusion of oxygen is ignored as in [1]. A derivation of the model, and discussion of its range of validity, can be found in Appendix A.

We are of course interested in solutions with $\rho \geq 0$ and $Y \geq 0$ everywhere. We consider (2.1) and (2.2) on $-\infty < x < \infty$, $t \geq 0$, with the constant boundary conditions

$$(\theta, \rho, Y)(-\infty) = (\theta^L, \rho^L, Y^L), \quad (\theta, \rho, Y)(\infty) = (\theta^R, \rho^R, Y^R). \tag{2.5}$$

We assume that the reaction does not occur at the boundaries, i.e. the reaction terms in (A.7)–(A.9) vanish. There are three reasons the reaction terms can vanish:

(1) Temperature control (TC) — reaction ceases due to low temperature $\theta \leq 0$;
(2) Fuel control (FC) — reaction ceases due to lack of fuel $\rho = 0$;
(3) Oxygen control (OC) — reaction ceases due to lack of oxygen $Y = 0$.

Of course, two or all three of these conditions can occur simultaneously. We limit ourselves to generic boundary conditions:

(L) Exactly one of the following conditions holds: $\theta^L \leq 0$, or $\rho^L = 0$, or $Y^L = 0$. The other two numbers are positive.
(R) Exactly one of the following conditions holds: $\theta^R \leq 0$, or $\rho^R = 0$, or $Y^R = 0$. The other two numbers are positive.

3. Combustion Waves

We denote by $(\theta^-, \rho^-, Y^-) \xrightarrow{c} (\theta^+, \rho^+, Y^+)$ a wave of velocity c that connects (θ^-, ρ^-, Y^-) at the left to (θ^+, ρ^+, Y^+) at the right. At the end states of the wave, the reaction terms in (A.7)–(A.9) vanish.

States at which the reaction terms vanish can be classified as TC, FC, OC, $TC \cap FC$, $TC \cap OC$, $FC \cap OC$, or $TC \cap FC \cap OC$. The type of the state indicates exactly which conditions hold at that state; for example, a $TC \cap FC$ state has $\theta \leq 0$, $\rho = 0$, and $Y > 0$. A wave of velocity c from a state of type $FC \cap OC$ to one of type TC, for example, would be indicated $FC \cap OC \xrightarrow{c} TC$. States other than TC, FC, and OC cannot be the first or last state of a wave sequence because of assumptions (L) and (R). However, as we shall see in Sec. 5, they cannot be ignored as possible intermediate states.

By a "combustion wave" we shall mean a continuous nontrivial traveling wave with velocity $c > 0$, $c \neq a$. We do not consider waves with velocity $c < 0$, since we have in mind injecting air into one end of a porous medium. Thus the spatial domain

would be $0 \le x < \infty$, so waves with negative velocity would not be supported. Waves with velocity $c = 0$ and $c = a$, the characteristic velocities of the system, are considered separately in the following section.

We are concerned especially with combustion waves that approach both end states exponentially. This limitation allows us to ignore certain waves that exist only when $\theta^+ = 0$, but approach the right state more slowly than exponentially. The consequence is that we can treat right states with $\theta^+ = 0$ exactly like right states with $\theta^+ < 0$. The limitation would also allow us to ignore traveling waves with $\theta^- = 0$, since it turns out that they necessarily approach the left state more slowly than exponentially. However, in this case, the traveling waves represent bifurcations that we find it helpful to understand. For other approaches see [1, 2, 5, 9, 18, 20].

Theorem 3.1. *There are exactly four types of combustion waves that approach both end states exponentially, two fast* (*wave velocity* $c_f > a$) *and two slow* (*positive wave velocity* $c_s < a$):

- $FC \xrightarrow{c_f} TC$.
- $OC \xrightarrow{c_f} TC$.
- $FC \xrightarrow{c_s} OC$
- $TC \xrightarrow{c_s} OC$.

In a fast combustion wave, the burning front moves toward a low-temperature region with both solid fuel and oxygen; this is often called "premixed combustion". The heat produced remains behind the combustion front because the moving gas that could transport it has lower velocity. Behind the front the reaction stops because the fuel is exhausted ($FC \xrightarrow{c_f} TC$), the oxygen is exhausted ($OC \xrightarrow{c_f} TC$), or both ($FC \cap OC \xrightarrow{c_f} TC$). We study these fronts in Sec. 7.

In a slow combustion wave, a gas bringing oxygen flows into a region in which solid fuel is present but oxygen is not. Combustion occurs behind the incoming gas; it cannot occur ahead since there is no oxygen. Thus the speed of the combustion front c cannot be greater than a. In fact $c < a$, so heat produced by combustion, which also moves with speed a, is swept ahead of the combustion front. Hence the high-temperature region is ahead of the front. The oxygen is entirely consumed in the reaction. These fronts have been called "reaction-trailing smolder waves" [18] and "coflow (or forward) filtration combustion waves" [2]. We study them in Sec. 8.

The following results describe the combustion waves.

Theorem 3.2 (Fast Combustion Waves). *Fix* $a > 0$. *Let* (θ^+, ρ^+, Y^+) *be a state of type TC, i.e.* $\theta^+ \le 0$, $\rho^+ > 0$, $Y^+ > 0$. *Assume in addition that* $\theta^+ + Y^+ > 0$. *Then there exist a state* (θ^-, ρ^-, Y^-) *and a velocity* $c_f > a$ *such that there is a combustion wave* $(\theta^-, \rho^-, Y^-) \xrightarrow{c_f} (\theta^+, \rho^+, Y^+)$ *that approaches its right state exponentially. It has* $\theta^- > 0$, *and* ρ^- *or* Y^- *or both equal to* 0. *More precisely, for fixed* (θ^+, ρ^+), *there is a unique* Y_*^+ *with* $\theta^+ + Y_*^+ > 0$ *such that*

(1) *if* $-\theta^+ < Y^+ < Y_*^+$, *then there exists a combustion wave of type* $OC \xrightarrow{c_f} TC$;

(2) *if* $Y^+ = Y^+_*$, *then there exists a combustion wave of type* $FC \cap OC \xrightarrow{c_f} TC$;
(3) *if* $Y^+ > Y^+_*$, *then there exists a combustion wave of type* $FC \xrightarrow{c_f} TC$.

In all cases, $\theta^+ + Y^+ = \theta^- + Y^-$ *and* $c_f = \frac{aY^+ - aY^-}{Y^+ - Y^- + \rho^- - \rho^+}$. *In the first and third cases the wave also approaches its left state exponentially; in the second case it does not. There are no combustion waves with* $c > a$ *and* $\theta^+ + Y^+ \leq 0$.

Theorem 3.2 says that if the right state has too little oxygen (i.e. if $\theta^+ + Y^+ \leq 0$), then the reaction cannot occur; if it has a moderate amount of oxygen, then there exists a combustion wave in which all the oxygen is used up in the reaction; and if it has lots of oxygen, then there exists a combustion wave in which all the fuel is used up in the reaction.

We conjecture that the combustion waves described in Theorem 3.2 are unique and depend smoothly on the right state, i.e. given $a > 0$, $\theta^+ \leq 0$, $\rho^+ > 0$, and $Y^+ > -\theta^+$, there is a unique $c > a$, given by a smooth function of (θ^+, ρ^+, Y^+), such that there is a combustion wave with velocity c and left state (θ^+, ρ^+, Y^+). In Sec. 9, we present numerical evidence for the uniqueness.

If this conjecture is true, then Theorem 3.2 describes a smooth mapping from the space of temperature-controlled right states, which has dimension 3 to the space of oxygen-controlled or fuel-controlled left states, which has dimension 2. By Sard's Theorem, almost every oxygen-controlled or fuel-controlled left state would correspond to a one-dimensional set of right states (which may be empty).

When the right state of a combustion wave is temperature-controlled, the oxygen concentration there, Y^+, is typically $\mathcal{O}(1)$. Thus the assumption $\theta^+ + Y^+ > 0$ holds whenever the temperature θ^+ at the right state is not too far below ignition temperature 0. This assumption is reasonable; in engineering it is often assumed that the two are equal.

Theorem 3.3 (Slow Combustion Waves). (1) $FC \xrightarrow{c_s} OC$ *and* $FC \cap TC \xrightarrow{c_s} OC$ *Waves. Fix* $a > 0$. *Let* $(\theta^-, 0, Y^-)$ *have* $\theta^- \geq 0$ *and* $Y^- > 0$. *Then for each* $\rho^+ > 0$, *there are unique numbers* $\theta^+ > 0$ *and* c_s, $0 < c_s < a$, *such that there exists a combustion wave of velocity* c_s *from* $(\theta^-, 0, Y^-)$ *to* $(\theta^+, \rho^+, 0)$. *In fact,*

$$\theta^+ = \theta^- + Y^-, \quad c_s = \frac{Y^-}{\rho^+ + Y^-} a. \tag{3.1}$$

These waves approach their right state exponentially, and approach their left state exponentially if and only if $\theta^- > 0$, *i.e. if and only if the left state is of type FC.*

(2) $TC \xrightarrow{c_s} OC$ *Waves. Fix* $a > 0$. *Let* $\theta^- < 0$, Y^- *with* $\theta^- + Y^- > 0$, *and* $\rho^+ > 0$ *be given. Then there are numbers* $\rho^- > 0$, $\theta^+ > 0$, *and* c_s, $0 < c_s < a$, *such that there exists a combustion wave of velocity* c_s *from* (θ^-, ρ^-, Y^-) *to* $(\theta^+, \rho^+, 0)$. *Moreover,* $\theta^+ = \theta^- + Y^-$, *and the quantities* c_s *and* ρ^- *are related*

by the formula

$$c_s = \frac{aY^-}{Y^- - \rho^- + \rho^+}.$$

These waves approach both end states exponentially.

(3) *There are no other combustion waves* $0 < c < a$. *In particular, there are no slow combustion waves with* $\theta^- + Y^- \le 0$.

Theorem 3.3(1) says that for each left state of type FC, and for the left state $(0, 0, Y^-)$ with $Y^- > 0$, there is a one-parameter family of right states of type OC to which the left state can be connected by a slow combustion wave.

On the other hand, Theorem 3.3(2) says that to have a slow combustion wave of speed c_s from a left state (θ^-, ρ^-, Y^-) of type TC to a right state $(\theta^+, \rho^+, 0)$ of type OC, the triple (θ^-, Y^-, ρ^+) may be chosen arbitrarily, and then a corresponding triple (ρ^-, θ^+, c_s) can be found. In Sec. 9, we present numerical evidence that the triple (ρ^-, θ^+, c_s) is unique.

The set of points in $(\theta^-, \rho^-, Y^-, \theta^+, \rho^+, c_s)$-space that corresponds to $TC \xrightarrow{c_s} OC$ waves should be a three-dimensional manifold. We have not shown this, but if it is true, then by Sard's Theorem, almost every left state corresponds to a set of isolated right states (which may be empty). We conjecture that in fact every left state corresponds to a unique right state.

4. Contact Discontinuities

When one simulates a system such as (A.7)–(A.9) on $-\infty < x < \infty$, one uses initial conditions that differ from the boundary data only on a finite interval. The computed solution then differs perceptibly from the boundary data on an interval of size $\mathcal{O}(t)$ because it includes waves that propagate with different velocities. In order to view the solution for fixed time on a computer screen, one must shrink the spatial interval by an $\mathcal{O}(t)$ factor. When one does this, combustion waves become steeper and approach discontinuities that propagate at velocity c and separate intervals on which (θ, ρ, Y) is constant. Other patterns of finite size, or even size $o(t)$, approach discontinuities that propagate at a characteristic velocity of the system and likewise separate intervals on which (θ, ρ, Y) is constant. We call these propagating discontinuities *contact discontinuities* because of their analogy to classical contact discontinuities, explained below. Since we are interested in the appearance of the solution for large time, we shall consider contact discontinuities in addition to combustion waves.

In the absence of reaction and diffusion terms, the characteristic velocities of (A.7)–(A.9) are 0 for the solid fuel and a for temperature and oxygen. Contact discontinuities therefore have velocity 0 or a. The solid fuel concentration can change across a contact discontinuity of velocity 0, while temperature or oxygen concentration or both can change across a contact discontinuity of velocity a. Contact

discontinuities must separate intervals on which the reaction does not occur (since (θ, ρ, Y) is constant).

To explain why we use the term "contact discontinuity", we note that on the portions of the solution that asymptotically approach contact discontinuities, the reaction has essentially stopped. If one removes the reaction terms from (A.7)–(A.9), the system decouples into

$$\partial_t \theta + a\partial_x \theta = \partial_{xx}\theta, \tag{4.1}$$

$$\partial_t \rho = 0, \tag{4.2}$$

$$\partial_t Y + a\partial_x Y = 0. \tag{4.3}$$

Equations (4.2) and (4.3) have solutions that are classical contact discontinuities: piecewise constant, where the discontinuity propagates with velocity 0 or a, respectively. Equation (4.1) is the heat equation together with convection with velocity a. A solution that approaches given values $\theta_\pm$ at $x = \pm\infty$ is

$$\theta(x,t) = \theta^- + \frac{1}{2}\left(1 + \operatorname{erf}\left(\frac{x - at}{\sqrt{4t}}\right)\right)(\theta^+ - \theta^-),$$

which is a widening wave of width $\mathcal{O}(t^{\frac{1}{2}})$. Since the width of the wave is $o(t)$, when the interval is shrunk by an $\mathcal{O}(t)$ factor, it will approach a piecewise constant discontinuity propagating with velocity a, i.e. a classical contact discontinuity of (4.1) with the diffusion term replace by 0.

In Sec. 5, we describe wave sequences that solve the BVP (2.1)–(2.5). We recall from Sec. 2 the assumption that at each end state, the reaction does not occur for one reason only. We shall consider only generic wave sequences, by which we mean the following. In six-dimensional $\theta^L\rho^L Y^L\theta^R\rho^R Y^R$-space, let B denote the set of allowed boundary conditions, i.e. the set of points that satisfy assumptions (L) and (R) of Sec. 2. A generic wave sequence is one that exists for an open set of parameter values in B.

The waves must occur in order of increasing velocity. It is easy to see that there is at most one slow combustion wave and one fast combustion wave. We may also assume:

(O) There is at most one wave of velocity 0 and one of velocity a.

The reason is that a sequence of two contact discontinuities with the same velocity could be combined into one.

The *dimension number* of a contact discontinuity is the dimension of the set of right states that can be reached from a fixed left state by a contact discontinuity of the given type. For example, for a contact discontinuity of speed 0, the ρ-component of the right state can be varied (dimension 1) unless it is 0 (dimension 0). For a contact discontinuity of speed a, both the θ- and Y-components of the right state can be varied (dimension 2), unless the Y-component of the right state is 0 (dimension 1).

Theorem 4.1. *With assumptions* (L), (R), *and* (O), *the contact discontinuities that occur in generic wave sequences are those given in Table* 1.

Table 1. Contact discontinuities.

Contact discontinuity	Dimension number
$TC \xrightarrow{0} TC$	1
$TC \xrightarrow{0} TC \cap FC$	0
$OC \xrightarrow{0} OC$	1
$OC \xrightarrow{0} FC \cap OC$	0
$TC \xrightarrow{a} TC$	2
$TC \xrightarrow{a} OC$	1
$FC \xrightarrow{a} FC$	2
$OC \xrightarrow{a} OC$	1
$OC \xrightarrow{a} TC$	2
$TC \cap FC \xrightarrow{a} FC$	2
$FC \cap OC \xrightarrow{a} FC$	2

We remark that four of the these contact discontinuities begin or end at states of type $TC \cap FC$ or $OC \cap FC$. By assumptions (L) and (R), these states cannot be the first or last in the wave sequence. They can, however, be intermediate states in generic wave sequences.

In the remainder of this section we show that contact discontinuities other than the given types cannot occur in generic wave sequences. In the following section we exhibit generic wave sequences that include all the contact discontinuities listed, thus completing the proof of Theorem 4.1.

Since a contact discontinuity of speed 0 must be the first wave in the sequence, by assumption (L) the left state is TC, FC, or OC. It cannot be FC: across a contact discontinuity of speed 0, ρ and only ρ changes, so the new right state would not be allowed. When the left state is TC or OC, after a change in ρ, the right state is of the same type as the left, or its type is that of the left state intersected with FC. Thus only the four contact discontinuities of speed 0 that are listed in the table can occur.

A contact discontinuity of speed a is either followed by a fast combustion wave, or is the last wave in the sequence. In the first case, by Theorem 3.1, its right state is of type FC or OC in a generic wave sequence; in the second case, by assumption (R), the right state is of type TC, FC, or OC. Thus, in a generic wave sequence, only contact discontinuities of speed a with right state of type TC, FC, or OC can occur.

In addition, contact discontinuities of speed a whose first state is $TC \cap OC$ or $TC \cap FC \cap OC$ cannot occur in a generic wave sequence. By assumption (L), such a wave cannot begin the wave sequence, and a look at the allowed slower waves shows that none end in one of these states.

There remain 15 possible contact discontinuities of speed a: five possible left states (TC, FC, OC, $TC \cap FC$, $FC \cap OC$) and three possible right states (TC, FC, OC). Eight cannot occur because a wave of speed a cannot remove or create the condition FC: $FC \xrightarrow{a} TC$, $FC \xrightarrow{a} OC$, $TC \cap FC \xrightarrow{a} TC$, $TC \cap FC \xrightarrow{a} OC$, $FC \cap OC \xrightarrow{a} TC$, $FC \cap OC \xrightarrow{a} OC$, $TC \xrightarrow{a} FC$, $TC \xrightarrow{a} OC$. The remaining seven are listed in the table.

5. Wave Sequences

Table 2 lists the four types of combustion waves in Theorem 3.1, together with their dimension numbers, which were explained in Sec. 3.

Table 2. Combustion waves.

Combustion wave	Dimension number
$FC \xrightarrow{c_f} TC$	1
$OC \xrightarrow{c_f} TC$	1
$FC \xrightarrow{c_s} OC$	1
$TC \xrightarrow{c_s} OC$	0

An obvious necessary condition for a wave sequence to be generic is that it begins at a state S^L of type TC, FC, or OC, and ends at a state S^R of type TC, FC, or OC. If S^R is of type FC ($\rho^R = 0$), there is a two-parameter family of states of the same type nearby obtained by varying θ^R and Y^R. Similarly, if S^R is of type OC, there is a two-parameter family of states of the same type nearby obtained by varying θ^R and ρ^R; and if S^R is of type TC, there is a three-parameter family of states of the same type nearby, since θ^R can be varied along with ρ^R and Y^R.

Thus a second necessary condition for a wave sequence from a left state S^L to a right state S^R to be generic is that for left states of the same type near S^L, the intermediate states of the wave sequence can be varied to arrive at

- a two-parameter family of states near S^R if S^R is of type FC or OC;
- a three-parameter family of states near S^R if S^R is of type TC.

It follows that for a wave sequence to be generic, the wave dimension numbers must sum to at least 2 if the right state is of type FC or OC, and to at least 3 if the right state is of type TC.

Figure 1 shows all possible sequences of the waves in Theorems 3.1 and 4.1 with (1) left state of type TC, FC, or OC, (2) increasing wave speed, and (3) sequences extended as far as possible. Wave dimension numbers are also indicated. From this figure one can read off all wave sequences with (1) left state of type TC, FC, or OC, (2) right state of type TC, FC, or OC, and (3) correct sum of the wave numbers. These 18 sequences are listed below; by giving the intermediate states explicitly we verify that they are in fact generic. Generic wave sequences ending at states of type

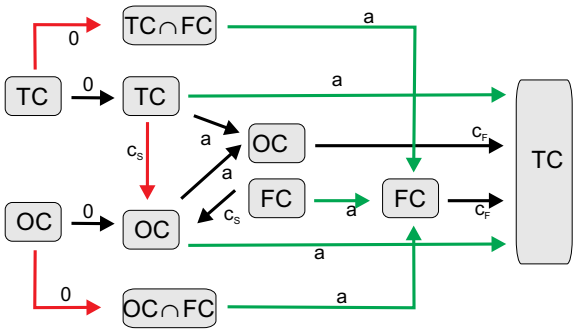

Fig. 1. (Color online) All possible sequences of the waves in Tables 1 and 2 with (1) left state of type TC, FC, or OC, (2) increasing wave speed, and (3) sequences extended as far as possible. Red arrow: dimension number 0. Black arrow: dimension number 1. Green arrow: dimension number 2.

FC or OC (respectively, TC) all have dimension number sum 2 (respectively, 3). Wave sequences with higher dimension number sum do not exist.

There are nine types of BVPs, depending on whether the left and right states are temperature-controlled (TC), fuel-controlled (FC), or oxygen-controlled (OC). We first give a brief summary of the possible wave sequences, followed by a detailed account for the interested reader.

(1) Fuel-controlled right state. A combustion wave moving right cannot occur because there is no fuel at the right and no mechanism to bring fuel to the right. Each possible left state gives rise to a unique sequence of contact discontinuities. Notice that this wave sequence represents the asymptotic state of the system. Combustion may occur for a while in certain regions (for example, regions where fuel, oxygen, and high temperature are initially present), but it eventually stops.

(2) Oxygen-controlled right state. Each possible left state again gives rise to a unique sequence of contact discontinuities, in which there are no combustion waves. In addition, fuel-controlled and temperature-controlled left states allow a wave sequence with a slow combustion wave (smoldering). When there is an oxygen-controlled right state, combustion must eventually die out unless oxygen is constantly brought to the right; this can only happen when the left state has a positive oxygen concentration.

(3) Temperature-controlled right state. Again each possible left state gives rise to a unique sequence of contact discontinuities, in which there are no combustion waves. In addition, there is a rich set of other possibilities.

- Each possible left state allows a wave sequence consisting of one or two contact discontinuities followed by a fast combustion wave. This is not surprising: the right state is "premixed", in that both oxygen and fuel are present. If combustion starts anywhere in the premixed region (because, for example,

a high temperature is initially present there), then the combustion process itself produces a wave of high temperature moving further into the premixed.

- A temperature-controlled left state allows a wave sequence in which there is a single slow combustion wave surrounded by contact discontinuities. The oxygen arriving from the left leads to a slow combustion wave preceded by a region of no oxygen: the oxygen arriving from the left all burned in the reaction, and the oxygen initially present at the right is carried away before the flame can reach it. Thus we have smoldering despite a premixed right state.
- Finally, temperature-controlled and oxygen-controlled left states each allow a wave sequence that includes both a slow and a fast combustion wave.

A detailed description of these wave sequences, along with simulation results, follows.

5.1. *Right state of type FC*

These BVPs do not permit combustion waves because there is no fuel at the right.

5.1.1. *TC to FC BVPs* ($\theta^L \leq 0$ *and* $\rho^R = 0$)

The only generic wave sequence is $TC \xrightarrow{0} TC \cap FC \xrightarrow{a} FC$; more precisely, $(\theta^L, \rho^L, Y^L) \xrightarrow{0} (\theta^L, 0, Y^L) \xrightarrow{a} (\theta^R, 0, Y^R)$. Notice that while we require assumptions (L) and (R) for the boundary conditions, a generic wave sequence can have an intermediate state at which the reaction fails to exist for two reasons.

5.1.2. *FC to FC BVPs* ($\rho^L = \rho^R = 0$)

The only generic wave sequence is a single $FC \xrightarrow{a} FC$ wave, namely $(\theta^L, 0, Y^L) \xrightarrow{a} (\theta^R, 0, Y^R)$.

5.1.3. *OC to FC BVPs* ($Y^L = 0$ *and* $\rho^R = 0$)

The only generic wave sequence is $OC \xrightarrow{0} FC \cap OC \xrightarrow{a} FC$; more precisely, $(\theta^L, \rho^L, 0) \xrightarrow{0} (\theta^L, 0, 0) \xrightarrow{a} (\theta^R, 0, Y^R)$.

5.2. *Right state of type OC*

These boundary conditions permit no combustion waves or only slow combustion waves.

5.2.1. *FC to OC BVPs* ($\rho^L = 0$, $Y^R = 0$)

The only generic wave sequence is $FC \xrightarrow{c_s} OC \xrightarrow{a} OC$. To construct the wave sequence, note that by Theorem 3.3, θ^L, Y^L, and ρ^R determine θ^N such that there

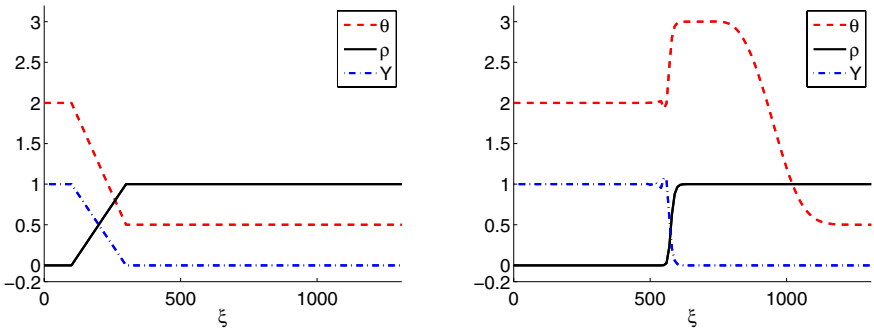

Fig. 2. Numerical simulation with $a = 5$ for the case described in Sec. 5.2.1, exhibiting a fuel-controlled to oxygen-controlled slow combustion wave followed by a contact discontinuity. Left: initial conditions. Right: simulation time 150. Notice that $\theta^+ \approx \theta^- + Y^-$ as predicted by Eq. (3.1) in Theorem 3.3. ($\theta^+ \approx 3.0$, $\theta^- = 2.0$, $Y^- = 1.0$.)

is a slow $FC \xrightarrow{c_s} OC$ combustion wave from $(\theta^L, 0, Y^L)$ to $(\theta^N, \rho^R, 0)$. This wave is followed by one of velocity a:

$$(\theta^L, 0, Y^L) \xrightarrow{c_s} (\theta^N, \rho^R, 0) \xrightarrow{a} (\theta^R, \rho^R, 0).$$

See the simulation result in Fig. 2. Notice that waves of speed 0 cannot exist when the left state is fuel-controlled; thus a wave sequence for an FC to OC BVP must have a combustion wave in which the fuel concentration changes from 0 to positive. Hot gas moves into a region where there is fuel; combustion then occurs.

5.2.2. *OC to OC BVPs* ($Y^L = Y^R = 0$)

The only generic wave sequence is $OC \xrightarrow{0} OC \xrightarrow{a} OC$; more precisely, $(\theta^L, \rho^L, 0) \xrightarrow{0} (\theta^L, \rho^R, 0) \xrightarrow{a} (\theta^R, \rho^R, 0)$.

5.2.3. *TC to OC BVPs* ($\theta^L \le 0$, $Y^R = 0$)

There are two generic wave sequences.

(1) $TC \xrightarrow{0} TC \xrightarrow{a} OC$; more precisely, $(\theta^L, \rho^L, Y^L) \xrightarrow{0} (\theta^L, \rho^R, Y^L) \xrightarrow{a} (\theta^R, \rho^R, 0)$. See the simulation result in Fig. 3.

(2) For $\theta^L + Y^L > 0$, $TC \xrightarrow{0} TC \xrightarrow{c_s} OC \xrightarrow{a} OC$. To construct the wave sequence, note that if $\theta^L + Y^L > 0$, then by Theorem 3.3, θ^L, Y^L, and ρ^R determine θ^N and ρ^M such that there is a slow $TC \xrightarrow{c_s} OC$ combustion wave from (θ^L, ρ^M, Y^L) to $(\theta^N, \rho^R, 0)$. The sequence is completed with waves of velocity 0 and a:

$$(\theta^L, \rho^L, Y^L) \xrightarrow{0} (\theta^L, \rho^M, Y^L) \xrightarrow{c_s} (\theta^N, \rho^R, 0) \xrightarrow{a} (\theta^R, \rho^R, 0).$$

See the simulation result in Fig. 4.

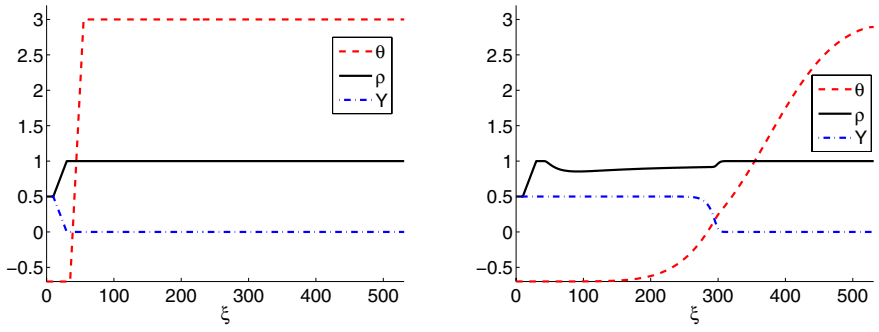

Fig. 3. Numerical simulation with $a = 0.1$ for the case (1) described in Sec. 5.2.3, exhibiting contact discontinuities of speeds 0 and a. Left: initial conditions. Right: simulation time 3500. Notice that $\theta^L + Y^L < 0$, which precludes combustion.

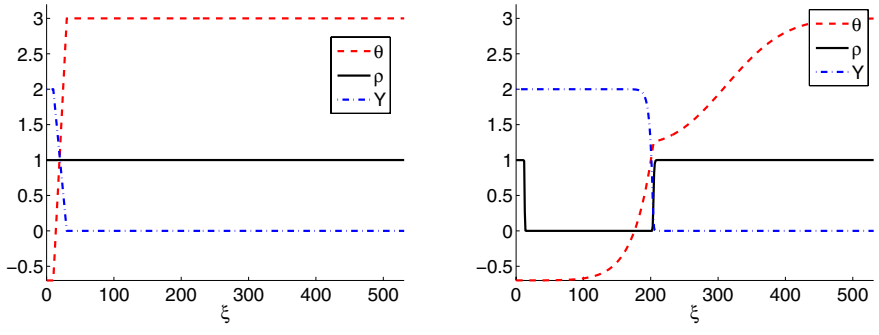

Fig. 4. Numerical simulation with $a = 0.1$ for the case (2) described in Sec. 5.2.3, exhibiting a temperature-controlled to oxygen-controlled slow combustion wave that is preceded and followed by contact discontinuities. Left: initial conditions. Right: simulation time 3000. Notice that $\theta^L + Y^L > 0$, which allows combustion. The temperature of combustion θ^+ is approximately $\theta^- + Y^-$ as predicted by Theorem 3.3. ($\theta^+ \approx 1.3$, $\theta^- = -0.3$, $Y^- = 2.0$.)

5.3. *Right state of type TC*

These boundary conditions are the only ones that allow fast combustion waves.

5.3.1. *TC to TC BVPs* ($\theta^L \leq 0$ *and* $\theta^R \leq 0$)

There are five generic wave sequences.

(1) $TC \xrightarrow{0} TC \xrightarrow{a} TC$; more precisely, $(\theta^L, \rho^L, Y^L) \xrightarrow{0} (\theta^L, \rho^R, Y^L) \xrightarrow{a} (\theta^R, \rho^R, Y^R)$.

(2) $TC \xrightarrow{0} TC \xrightarrow{c_s} OC \xrightarrow{a} TC$; more precisely, $(\theta^L, \rho^L, Y^L) \xrightarrow{0} (\theta^L, \rho^M, Y^L) \xrightarrow{c_s} (\theta^N, \rho^R, 0) \xrightarrow{a} (\theta^R, \rho^R, Y^R)$ (requires $\theta^L + Y^L > 0$). In the slow $TC \xrightarrow{c_s} OC$ combustion wave type, θ^L, Y^L, and ρ^R determine ρ^M and θ^N (Theorem 3.3). See the simulation result in Fig. 5.

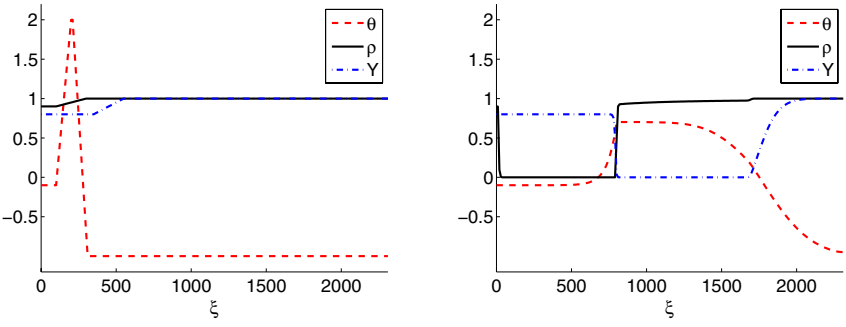

Fig. 5. Numerical simulation with $a = 0.1$ for the case (2) described in Sec. 5.3.1, exhibiting a temperature-controlled to oxygen-controlled slow combustion wave that is preceded and followed by contact discontinuities. Left: initial conditions. Right: simulation time 14,000.

(3) By Theorem 3.2, given (θ^R, ρ^R, Y^R), there exists (θ^N, ρ^N, Y^N), with $\theta^N > 0$ and ρ^N or Y^N equal to 0, such that there is a fast $FC \xrightarrow{c_f} TC$ or $OC \xrightarrow{c_f} TC$ combustion wave from (θ^N, ρ^N, Y^N) to (θ^R, ρ^R, Y^R). There are then two possibilities.

(a) $\rho^N = 0$: $TC \xrightarrow{0} TC \cap FC \xrightarrow{a} FC \xrightarrow{c_f} TC$; more precisely, $(\theta^L, \rho^L, Y^L) \xrightarrow{0} (\theta^L, 0, Y^L) \xrightarrow{a} (\theta^N, 0, Y^N) \xrightarrow{c_f} (\theta^R, \rho^R, Y^R)$.

(b) $Y^N = 0$: Again two possibilities:

(i) $TC \xrightarrow{0} TC \xrightarrow{a} OC \xrightarrow{c_f} TC$; more precisely, $(\theta^L, \rho^L, Y^L) \xrightarrow{0} (\theta^L, \rho^N, Y^L) \xrightarrow{a} (\theta^N, \rho^N, 0) \xrightarrow{c_f} (\theta^R, \rho^R, Y^R)$.

(ii) $TC \xrightarrow{0} TC \xrightarrow{c_s} OC \xrightarrow{a} OC \xrightarrow{c_f} TC$ (requires $\theta^L + Y^L > 0$). To construct the wave sequence, note that if $\theta^L + Y^L > 0$, then by Theorem 3.3, θ^L, Y^L, and ρ^N determine ρ^M and θ^M such that there is a slow $TC \xrightarrow{c_s} OC$ combustion wave from (θ^L, ρ^M, Y^L) to $(\theta^M, \rho^N, 0)$. The sequence is completed with waves of speed 0 and a:

$$(\theta^L, \rho^L, Y^L) \xrightarrow{0} (\theta^L, \rho^M, Y^L) \xrightarrow{c_s} (\theta^M, \rho^N, 0) \xrightarrow{a} (\theta^N, \rho^N, 0) \xrightarrow{c_f} (\theta^R, \rho^R, Y^R).$$

5.3.2. *FC to TC BVPs* ($\rho^L = 0$, $\theta^R \le 0$)

There are three generic wave sequences.

(1) $FC \xrightarrow{c_s} OC \xrightarrow{a} TC$. To construct the wave sequence, note that by Theorem 3.3, θ^L, Y^L, and ρ^R determine θ^M such that there is a slow $FC \xrightarrow{c_s} OC$ combustion wave from $(\theta^L, 0, Y^L)$ to $(\theta^M, \rho^R, 0)$. The variables θ and Y are then adjusted by a wave of speed a:

$$(\theta^L, 0, Y^L) \xrightarrow{c_s} (\theta^M, \rho^R, 0) \xrightarrow{a} (\theta^R, \rho^R, Y^R).$$

See the simulation result in Fig. 6.

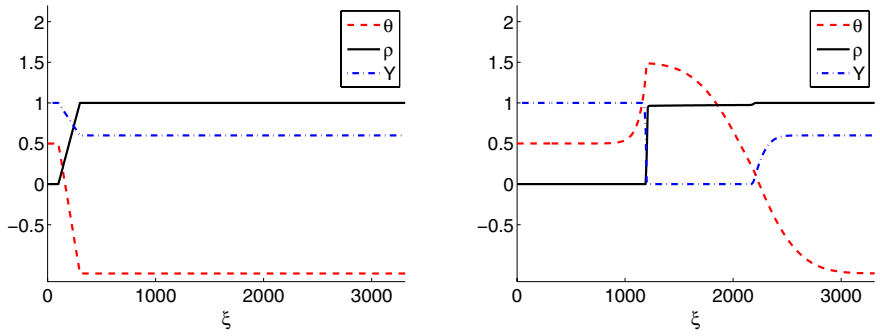

Fig. 6. Numerical simulation with $a = 0.1$ for the case (1) described in Sec. 5.3.2, exhibiting a fuel-controlled to oxygen-controlled slow combustion wave followed by a contact discontinuity. Left: initial conditions. Right: simulation time 20,000.

(2) By Theorem 3.2, given (θ^R, ρ^R, Y^R), there exists (θ^N, ρ^N, Y^N), with $\theta^N > 0$ and ρ^N or Y^N equal to 0, such that there is a fast $FC \xrightarrow{c_f} TC$ or $OC \xrightarrow{c_f} TC$ combustion wave from (θ^N, ρ^N, Y^N) to (θ^R, ρ^R, Y^R). There are then two possibilities.

(a) $\rho^N = 0$: $FC \xrightarrow{a} FC \xrightarrow{c_f} TC$; more precisely, $(\theta^L, 0, Y^L) \xrightarrow{a} (\theta^N, 0, Y^N) \xrightarrow{c_f} (\theta^R, \rho^R, Y^R)$. See the simulation result in Fig. 7.

(b) $Y^N = 0$: $FC \xrightarrow{c_s} OC \xrightarrow{a} OC \xrightarrow{c_f} TC$. To construct the wave sequence, note that by Theorem 3.3, θ^L, Y^L, and ρ^N determine θ^M such that there is a slow $FC \xrightarrow{c_s} OC$ combustion wave from $(\theta^L, 0, Y^L)$ to $(\theta^M, \rho^N, 0)$. Between the slow and fast combustion waves there is a wave of velocity a:

$$(\theta^L, 0, Y^L) \xrightarrow{c_s} (\theta^M, \rho^N, 0) \xrightarrow{a} (\theta^N, \rho^N, 0) \xrightarrow{c_f} (\theta^R, \rho^R, Y^R).$$

See the simulation result in Fig. 8.

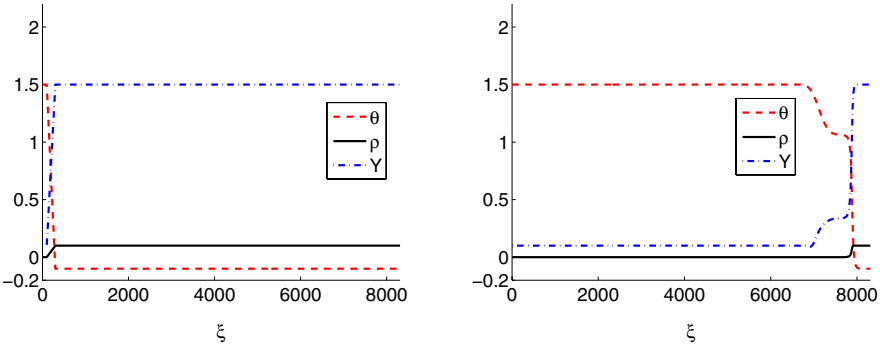

Fig. 7. Numerical simulation with $a = 5$ for the case (2)(a) described in Sec. 5.3.2, exhibiting a fuel-controlled to temperature-controlled fast combustion wave preceded by a contact discontinuity. Left: initial conditions. Right: simulation time 450.

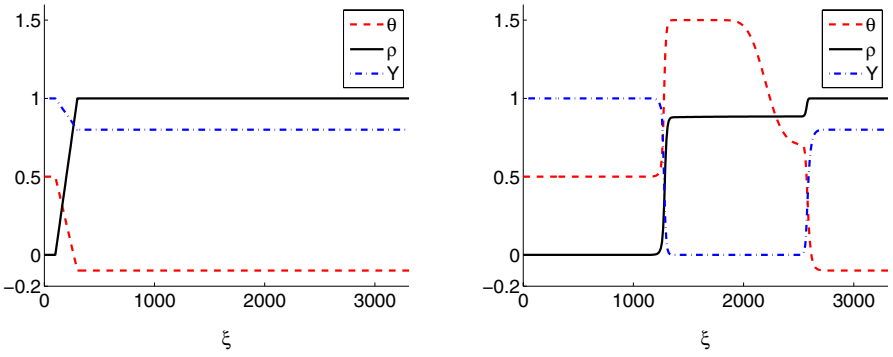

Fig. 8. Numerical simulation with $a = 5$ for the case (2)(b) described in Sec. 5.3.2, exhibiting slow (fuel-controlled to oxygen-controlled) and fast (oxygen-controlled to temperature-controlled) combustion waves surrounding a contact discontinuity. Left: initial conditions. Right: simulation time 400. Notice that $\theta^+ \approx \theta^- + Y^-$ as predicted by Theorem 3.3.

5.3.3. *OC to TC BVPs* ($Y^L = 0$, $\theta^R \leq 0$)

There are three generic wave sequences.

(1) $OC \xrightarrow{0} OC \xrightarrow{a} TC$; more precisely, $(\theta^L, \rho^L, 0) \xrightarrow{0} (\theta^L, \rho^R, 0) \xrightarrow{a} (\theta^R, \rho^R, Y^R)$.

(2) By Theorem 3.2, given (θ^R, ρ^R, Y^R), there exists (θ^N, ρ^N, Y^N), with $\theta^N > 0$ and ρ^N or Y^N equal to 0, such that there is a fast $FC \xrightarrow{c_f} TC$ or $OC \xrightarrow{c_f} TC$ combustion wave from (θ^N, ρ^N, Y^N) to (θ^R, ρ^R, Y^R). There are then two generic wave sequences:

(a) $\rho^N = 0$: $OC \xrightarrow{0} FC \cap OC \xrightarrow{a} FC \xrightarrow{c_f} TC$; more precisely,

$$(\theta^L, \rho^L, 0) \xrightarrow{0} (\theta^L, 0, 0) \xrightarrow{a} (\theta^N, 0, Y^N) \xrightarrow{c_f} (\theta^R, \rho^R, Y^R).$$

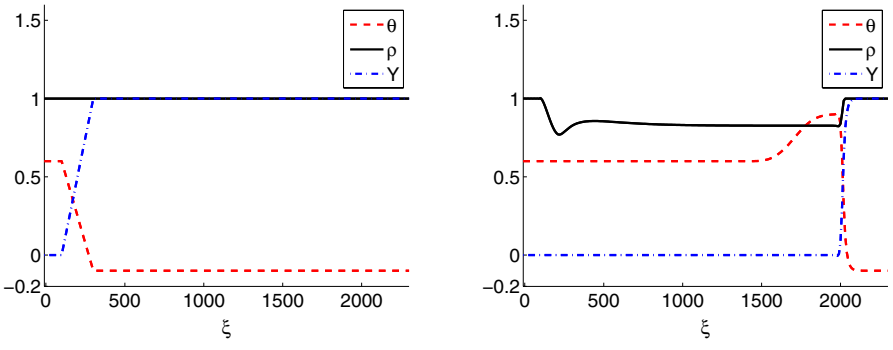

Fig. 9. Numerical simulation with $a = 5$ for the case (2)(b) described in Sec. 5.3.3, exhibiting an oxygen-controlled to temperature-controlled fast combustion wave preceded by two contact discontinuities. Left: initial conditions. Right: simulation time 300.

(b) $Y^N = 0$: $OC \xrightarrow{0} OC \xrightarrow{a} OC \xrightarrow{c_f} TC$; more precisely,

$$(\theta^L, \rho^L, 0) \xrightarrow{0} (\theta^L, \rho^N, 0) \xrightarrow{a} (\theta^N, \rho^N, 0) \xrightarrow{c_f} (\theta^R, \rho^R, Y^R).$$

See the simulation result in Fig. 9.

For all simulations shown in this section we use nonlinear Crank–Nicolson implicit finite difference scheme and Newton's method in each time-step with $a = 5$.

The remainder of the paper is devoted to proving the results about combustion waves in Sec. 3. In Sec. 6, we derive a traveling wave equation suitable for analysis and we analyze its equilibria, which determine the possible connecting orbits. In Secs. 7 and 8, we find the connecting orbits.

6. Reduced Traveling Wave Equation

In order to most conveniently find the combustion waves of the system (2.1) and (2.3), we replace (2.2) by the sum of (2.2) and (2.1), and we replace (2.3) by the difference of (2.3) and (2.2). We obtain

$$\partial_t \theta + a\partial_x \theta = \partial_{xx}\theta + \rho Y \Phi(\theta), \tag{6.1}$$

$$\partial_t(\theta + \rho) + a\partial_x \theta = \partial_{xx}\theta, \tag{6.2}$$

$$\partial_t(Y - \rho) + a\partial_x Y = 0. \tag{6.3}$$

In (6.1)–(6.3), we replace the spatial coordinate x with one ξ that is moving with velocity c: $\xi = x - ct$. We obtain

$$\partial_t \theta = (c - a)\partial_\xi \theta + \partial_{\xi\xi}\theta + \rho Y \Phi(\theta), \tag{6.4}$$

$$\partial_t(\theta + \rho) = (c - a)\partial_\xi \theta + \partial_{\xi\xi}\theta + c\partial_\xi \rho, \tag{6.5}$$

$$\partial_t(Y - \rho) = (c - a)\partial_\xi Y - c\partial_\xi \rho. \tag{6.6}$$

A stationary solution of (6.4)–(6.6) is a traveling wave solution of (2.1)–(2.3) with velocity c. Stationary solutions of (6.4)–(6.6) satisfy the system of ODEs

$$0 = (c - a)\partial_\xi \theta + \partial_{\xi\xi}\theta + \rho Y \Phi(\theta), \tag{6.7}$$

$$0 = (c - a)\partial_\xi \theta + \partial_{\xi\xi}\theta + c\partial_\xi \rho, \tag{6.8}$$

$$0 = (c - a)\partial_\xi Y - c\partial_\xi \rho. \tag{6.9}$$

In (6.7), we set $v_1 = \partial_\xi \theta$, and we integrate (6.8) and (6.9). Using dot to denote derivative with respect to ξ, we obtain the system

$$\dot{\theta} = v_1, \tag{6.10}$$

$$\dot{v}_1 = (a - c)v_1 - \rho Y \Phi(\theta), \tag{6.11}$$

$$w_1 = (c - a)\theta + v_1 + c\rho, \tag{6.12}$$

$$w_2 = (c - a)Y - c\rho, \tag{6.13}$$

where w_1 and w_2 are constants.

We assume $c \neq a$. Then we can solve for Y using (6.13), and we solve for v_1 using (6.12). Substituting into (6.10) and (6.11) and dividing the second equation by c (we recall the standing assumption that $c > 0$), we obtain the reduced traveling wave system

$$\dot{\theta} = (a - c)\theta - c\rho + w_1, \tag{6.14}$$

$$\dot{\rho} = \frac{c\rho + w_2}{c(c - a)}\rho\Phi(\theta), \tag{6.15}$$

in which (w_1, w_2) is a vector of parameters. Because of (6.13), for the system (6.14) and (6.15),

$$\text{the point } (\theta, \rho) \text{ has } Y = \frac{c\rho + w_2}{c - a}. \tag{6.16}$$

The system (6.14) and (6.15) has the invariant lines

$$\rho = 0 \quad \text{and} \quad \rho = -\frac{w_2}{c};$$

the latter corresponds to $Y = 0$.

The physically relevant part of the phase space for (6.14) and (6.15), which we denote P, has $\rho \geq 0$ and $Y \geq 0$. From (6.16),

$$\text{if } 0 < c < a, \quad Y \geq 0 \text{ if and only if } \rho \leq -\frac{w_2}{c}; \tag{6.17}$$

$$\text{if } c > a, \quad Y \geq 0 \text{ if and only if } \rho \geq -\frac{w_2}{c}. \tag{6.18}$$

In the first case, P is nonempty if $w_2 \leq 0$; $P = \{(\theta, \rho) : 0 \leq \rho \leq -\frac{w_2}{c}\}$. In the second case, $P = \{(\theta, \rho) : \rho \geq \max(0, -\frac{w_2}{c})\}$. In both cases P is invariant.

The set of equilibria of (6.14) and (6.15) is the union of three subsets:

$$FC = \{(\theta, \rho) : \theta > 0, \rho = 0, c\rho + w_2 > 0, \text{and } (a - c)\theta - c\rho + w_1 = 0\},$$

$$OC = \{(\theta, \rho) : \theta > 0, \rho > 0, c\rho + w_2 = 0, \text{and } (a - c)\theta - c\rho + w_1 = 0\},$$

$$FC \cap OC = \{(\theta, \rho) : \theta > 0, \rho = 0, c\rho + w_2 = 0, \text{and } (a - c)\theta - c\rho + w_1 = 0\}.$$

$$TC^* = \{(\theta, \rho) : \theta \leq 0 \text{ and } (a - c)\theta - c\rho + w_1 = 0\}.$$

FC, OC, and $FC \cap OC$ consist of equilibria of those types only (recall (6.16)). TC^* includes equilibria of types TC, $TC \cap FC$, $TC \cap OC$, and $TC \cap FC \cap OC$, i.e. all low-temperature equilibria.

All equilibria lie on the line H defined by $(a - c)\theta - c\rho + w_1 = 0$. H has positive slope if $0 < c < a$ and negative slope if $c > a$. In terms of the natural variables (θ, v_1, ρ, Y), with $v_1 = \dot{\theta}$, H corresponds to $v_1 = 0$. The portion of H in $\theta \leq 0$ is TC; the portion in $\theta > 0$ is the disjoint union of FC ($\rho = 0$ only), OC ($Y = 0$ only), and $FC \cap OC$ ($\rho = Y = 0$).

The linearization of (6.14) and (6.15) at a point (θ, ρ) has the matrix

$$\begin{pmatrix} a-c & -c \\ \dfrac{c\rho + w_2}{c(c-a)}\rho\Phi'(\theta) & \dfrac{2c\rho + w_2}{c(c-a)}\Phi(\theta) \end{pmatrix}. \tag{6.19}$$

If $(\theta, \rho) \in TC^*$, (6.19) becomes

$$\begin{pmatrix} a-c & -c \\ 0 & 0 \end{pmatrix}. \tag{6.20}$$

Proposition 6.1. *At an equilibrium in TC^*, one eigenvalue is $a - c$, with eigenvector $(1, 0)$; the other eigenvalue is 0.*

If $(\theta, \rho) \in FC$ or $FC \cap OC$, (6.19) becomes

$$\begin{pmatrix} a-c & -c \\ 0 & \dfrac{w_2}{c(c-a)}\Phi(\theta) \end{pmatrix}. \tag{6.21}$$

We have $\rho = 0$. In FC, $Y > 0$, so

$$w_2 = (c-a)Y - c\rho = (c-a)Y \text{ has the sign of } c - a.$$

In $FC \cap OC$, $Y = 0$, so $w_2 = 0$. Therefore, we have the following proposition.

Proposition 6.2. *At an equilibrium in FC or $FC \cap OC$, one eigenvalue is $a - c$, with eigenvector $(1, 0)$. This eigenvector points along the invariant line $\rho = 0$. The other eigenvalue is positive in FC and 0 in $FC \cap OC$. Its eigenvector is transverse to the invariant line.*

If $(\theta, \rho) \in OC$, (6.19) becomes

$$\begin{pmatrix} a-c & -c \\ 0 & \dfrac{w_2}{c(a-c)}\Phi(\theta) \end{pmatrix}. \tag{6.22}$$

Since $\rho > 0$ and $c\rho + w_2 = 0$, we have $w_2 < 0$. Therefore, we have the following proposition.

Proposition 6.3. *An equilibrium in OC is a saddle. One eigenvalue is $a - c$, with eigenvector $(1, 0)$. This eigenvector points along the invariant line $\rho = -w_2/c$, which corresponds to $Y = 0$. The other eigenvector is transverse to the invariant line.*

The invariant lines $\rho = -\frac{w_2}{c}$ and $\rho = 0$ each contain just one equilibrium, so they do not contain traveling waves with finite limits at both ends. Therefore, from the propositions of this section we conclude that to find solutions of (6.14) and (6.15) that approach their end states exponentially, only the following cases need be considered:

- $0 < a < c$, left state in FC or OC, right state in TC^*.
- $0 < c < a$, left state in FC or TC^*, right state in OC.

7. Fast Traveling Waves ($c > a$)

In this section, we shall prove Theorem 3.2. In order to simplify the notation we use $(u_1, u_2, u_3) = (\theta, \rho, Y)$ in this section and the next.

We assume $c > a$. From Sec. 6, we assume that the right state of a traveling wave for (2.1)–(2.3) is (u_{1+}, u_{2+}, u_{3+}) with $u_{1+} \leq 0$. Since a wave with speed c_f will be the last wave in a wave sequence, we invoke assumption (R) to restrict our attention to $u_{2+} > 0$ and $u_{3+} > 0$, i.e. to right states in TC. Waves with other right states in TC^* cannot occur, but we will not bother to show it. It is obvious on physical grounds: if fuel is missing at the right, it cannot be transported there; if oxygen is missing at the right, it cannot be transported there fast enough to support a combustion wave with velocity greater than a.

The state (u_{1+}, u_{2+}, u_{3+}) corresponds to $(u_1, v_1, u_2, u_3) = (u_{1+}, 0, u_{2+}, u_{3+})$ and to

$$(u_1, u_2, w_1, w_2) = (u_{1+}, u_{2+}, (c-a)u_{1+} + cu_{2+}, (c-a)u_{3+} - cu_{2+}).$$

Therefore, in (6.14) and (6.15) we set

$$(w_1, w_2) = ((c-a)u_{1+} + cu_{2+}, (c-a)u_{3+} - cu_{2+}), \tag{7.1}$$

and obtain

$$\dot{u}_1 = (a-c)(u_1 - u_{1+}) - c(u_2 - u_{2+}), \tag{7.2}$$

$$\dot{u}_2 = \left(\frac{u_2 - u_{2+}}{c-a} + \frac{u_{3+}}{c}\right) u_2 \Phi(u_1). \tag{7.3}$$

The invariant line $u_3 = 0$ corresponds to

$$u_2 = -\frac{w_2}{c} = u_{2+} - \frac{c-a}{c} u_{3+}. \tag{7.4}$$

Since $c > a$, this line lies below $u_2 = u_{2+}$. It lies above (respectively, below) $u_2 = 0$ provided $u_{2+} > \frac{c-a}{c} u_{3+}$ (respectively, $u_{2+} < \frac{c-a}{c} u_{3+}$). The lines $u_2 = 0$ and $u_3 = 0$ coincide provided $u_{2+} = \frac{c-a}{c} u_{3+}$, i.e. $c = \frac{a u_{3+}}{u_{3+} - u_{2+}}$.

The system (7.2) and (7.3) has the vector of parameters $(a, c, u_1^+, u_2^+, u_3^+)$. For fixed (a, u_1^+, u_2^+) with $a > 0$, $u_1^+ \leq 0$, and $u_{2+} > 0$, we let

$$C = \left\{(u_{3+}, c) : u_{2+} < u_{3+} < \infty \text{ and } c = \frac{a u_{3+}}{u_{3+} - u_{2+}}\right\},$$

$$\text{Region 1} = \left\{(u_{3+}, c) : u_{2+} < u_{3+} < \infty \text{ and } c > \frac{a u_{3+}}{u_{3+} - u_{2+}}\right\},$$

$$\text{Region 2} = \{(u_{3+}, c) : u_{3+} > 0, c > a, \text{and } (u_{3+}, c) \notin C \cup \text{Region 1}\}.$$

See Fig. 10.

In the remainder of this section, we study the curve C (Proposition 7.1), Region 1 (Proposition 7.2), and Region 2 (Proposition 7.3). The three propositions of this section imply Theorem 3.2.

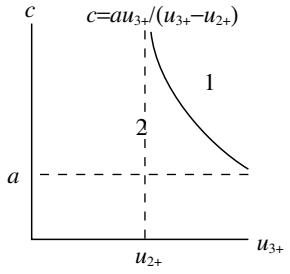

Fig. 10. Parameters for the fast traveling wave equation.

7.1. *The curve C*

On C, the lines $u_2 = 0$ and $u_3 = 0$ coincide.

Substituting $c = \frac{au_{3+}}{u_{3+}-u_{2+}}$ into (7.2) and (7.3) and multiplying the right-hand side by $au_{2+}(u_{3+} - u_{2+}) > 0$ (equivalent to a rescaling of time), we obtain

$$\dot{u}_1 = a^2 u_{2+}(u_{2+}(u_{1+} - u_1) + u_{3+}(u_{2+} - u_2)), \tag{7.5}$$

$$\dot{u}_2 = (u_{3+} - u_{2+})^2 u_2^2 \Phi(u_1). \tag{7.6}$$

See Fig. 11. Notice that where $u_2 > 0$, $\dot{u}_2 = 0$ for $u_1 \leq 0$ and $\dot{u}_2 > 0$ for $u_1 > 0$. The derivative $\dot{u}_1$ changes from positive to negative when the nullcline $u_{2+}(u_{1+} - u_1) + u_{3+}(u_{2+} - u_2) = 0$ is crossed from left to right.

The equilibrium (u_{1+}, u_{2+}) has a one-dimensional stable manifold.

If $u_{1+} + u_{3+} \leq 0$, there are no traveling waves with right state (u_{1+}, u_{2+}). If $u_{1+} + u_{3+} > 0$, the equilibrium $(u_{1+} + u_{3+}, 0)$ is in $FC \cap OC$ since $u_2 = u_3 = 0$. In $u_2 > 0$ it has a unique one-dimensional center manifold $W^c(u_{1+} + u_{3+}, 0)$, along which solutions in $u_2 > 0$ leave it. This curve is tangent to and above the isocline $u_{2+}(u_{1+} - u_1) + u_{3+}(u_{2+} - u_2) = 0$.

Proposition 7.1. *Let $a > 0$ and $u_{1+} \leq 0$.*

(1) *Suppose $u_{2+} \geq -u_{1+}$. Then there is a unique u_{3*}, $u_{2+} < u_{3*} < \infty$ such that, for* (7.5) *and* (7.6), *the stable manifold of (u_{1+}, u_{2+}) contains a branch of the*

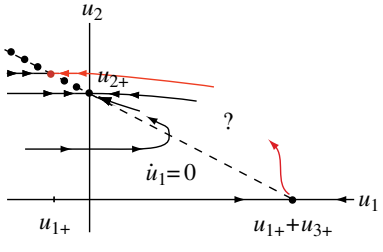

Fig. 11. Phase portrait of (7.5) and (7.6) in P ($u_2 \geq 0$) assuming $u_{1+} + u_{3+} > 0$.

center manifold of $(u_{1+} + u_{3*}, 0)$. *For* $u_{2+} < u_{3+} < u_{3*}$, *the former lies above the latter*; *for* $u_{3*} < u_{3+} < \infty$, *the former lies below the latter.*

(2) *Suppose* $u_{2+} < -u_{1+}$. *Then there is a unique* u_{3*}, $-u_{1+} < u_{3*} < \infty$ *such that, for* (7.5) *and* (7.6), *the stable manifold of* (u_{1+}, u_{2+}) *contains a branch of the center manifold of* $(u_{1+} + u_{3*}, 0)$. *For* $-u_{1+} < u_{3+} < u_{3*}$, *the former lies above the latter*; *for* $u_{3*} < u_{3+} < \infty$, *the former lies below the latter.*

The connection that exists for $u_{3+} = u_{3*}$ represents a combustion wave for (2.1)–(2.3) of type $FC \cap OC \xrightarrow{c_f} TC$. It does not approach its left state exponentially.

Proof of Proposition 7.1. In both cases of the proposition we only consider $u_{3+} > -u_1+$, so the phase portrait is given by Fig. 11.

In case (1) we consider the limit $u_{3+} = u_{2+}$ of (7.5) and (7.6). We obtain

$$\dot{u}_1 = a^2(u_{2+})^2((u_{1+} - u_1) + (u_{2+} - u_2)), \tag{7.7}$$

$$\dot{u}_2 = 0. \tag{7.8}$$

The line $(u_1 - u_{1+}) + (u_2 - u_{2+}) = 0$ is a line of normally attracting equilibria. The stable manifolds of points on this line are horizontal lines. In particular, the stable manifold of (u_{1+}, u_{2+}) is the line $u_2 = u_{2+}$, and the center manifold of $(u_{1+} + u_{3+}, 0) = (u_{1+} + u_{2+}, 0)$ is the line $(u_1 - u_{1+}) + (u_2 - u_{2+}) = 0$, $u_{1+} < u_1$. It follows that for u_{3+} a little larger than u_{2+}, the former lies above the latter.

In case (2) the corresponding limit $u_{3+} = -u_{1+}$. It leads to a similar conclusion, which is left to the reader.

Next we show that in either case, for u_{3+} large, there are orbits that start on the nullcline $u_{2+}(u_{1+} - u_1) + u_{3+}(u_{2+} - u_2) = 0$ that separate the stable manifold of (u_{1+}, u_{2+}) from the center manifold of $(u_{1+} + u_{3+}, 0)$. Thus the former lies below the latter.

To see this, fix ϵ, $0 < \epsilon < u_{2+}$, and consider (7.5) and (7.6) on the region $-u_{1+} + \epsilon \le u_1 \le -u_{1+} + 2\epsilon$, $u_{2+} - \epsilon \le u_2 \le u_{2+}$. On this region,

$$\frac{du_1}{du_2} = \frac{a^2 u_{2+}}{(u_{3+} - u_{2+})^2} \cdot \frac{u_{2+}(u_{1+} - u_1) + u_{3+}(u_{2+} - u_2)}{u_2^2 \Phi(u_1)}.$$

Therefore, on the given region,

$$\frac{a^2 u_{2+}}{(u_{3+} - u_{2+})^2} \cdot \frac{u_{2+}(2u_{1+} - 2\epsilon)}{(u_{2+} - \epsilon)^2 \rho(-u_{1+} + \epsilon)} \le \frac{du_1}{du_2} \le \frac{a^2 u_{2+}}{(u_{3+} - u_{2+})^2} \cdot \frac{u_{2+}(2u_{1+} - \epsilon) + u_{3+}\epsilon}{(u_{2+} - \epsilon)^2 \rho(-u_{1+} + \epsilon)}.$$

(The lower bound is negative and the upper bound is positive.) As $u_{3+} \to \infty$, both the lower bound and the upper bound approach 0. The result follows.

Therefore, for (7.5) and (7.6), there exists u_{3*}, with $u_{2+} < u_{3*} < \infty$ in case (1) and $-u_{1+} < u_{3*} < \infty$ in case (2), such that, for (7.5) and (7.6), the stable manifold of (u_{1+}, u_{2+}) contains a branch of the center manifold of $(u_{1+} + u_{3*}, 0)$.

The splitting of these manifolds for (7.5) and (7.6) as u_{3+} varies is governed by a Melnikov integral. (This is correct here even though the equilibria are degenerate; see [16].) Let $X(u_1, u_2) = (X_1(u_1, u_2), X_2(u_1, u_2))$ be the vector field given by the right-hand side of (7.5) and (7.6). Let u_{3+} be a value for which the connection exists, let $(u_1, u_2)(\tau)$ be the connecting orbit, and let $r(\tau) = \mathrm{div} X(u_1, u_2)(\tau)$. Then the Melnikov integral is given by

$$\begin{aligned} M &= \int_{-\infty}^{\infty} \exp\left[-\int_0^\tau r(\eta)d\eta\right] (-\dot{u}_2 \quad \dot{u}_1) \frac{\partial}{\partial u_{3+}} \begin{pmatrix} X_1 \\ X_2 \end{pmatrix} d\tau \\ &= \int_{-\infty}^{\infty} \exp\left[-\int_0^\tau r(\eta)d\eta\right] (-\dot{u}_2 \quad \dot{u}_1) \begin{pmatrix} a^2 u_{2+}(u_{2+} - u_2) \\ 2(u_{3+} - u_{2+})u_2^2 \Phi(u_1) \end{pmatrix} d\tau \\ &= \int_{-\infty}^{\infty} \exp\left[-\int_0^\tau r(\eta)d\eta\right] (2(u_{3+} - u_{2+})u_2^2 \Phi(u_1)\dot{u}_1 - a^2 u_{2+}(u_{2+} - u_2)\dot{u}_2) d\tau \\ &< 0 \end{aligned}$$

because $u_{2+} - u_2 > 0$, $\dot{u}_2 > 0$, and $\dot{u}_1 < 0$. Since $M < 0$, the center manifold of $(u_{1+} + u_{3+}, 0)$ crosses from below to above the stable manifold of (u_{1+}, u_{2+}) as u_{3+} increases past u_{3*}. Since this is true for any u_{3*} where the manifolds meet, it follows that u_{3*} is unique. □

7.2. *Region* 1

In Region 1, the line $u_3 = 0$ lies below $u_2 = 0$. See Fig. 12. A traveling wave with right state (u_{1+}, u_{2+}) exists if the unstable manifold of $(u_{1+} + \frac{c}{c-a}u_{2+}, 0)$ meets the stable manifold of equilibrium (u_{1+}, u_{2+}).

Proposition 7.2. *Let $a > 0$ and $u_{1+} \le 0$. Let u_{3*} given by Proposition* 7.1.

(1) *Suppose $u_{2+} \ge -u_{1+}$. For $u_{3*} < u_{3+} < \infty$, all points (u_{3+}, c) in Region* 1 *have $u_{1+} + \frac{c}{c-a}u_{2+} > 0$, so the phase portrait of* (7.2) *and* (7.3) *is given by Fig.* 12. *For each such u_{3+} there exists a velocity c, $\frac{au_{3+}}{u_{3+}-u_{2+}} < c < \infty$, such that the*

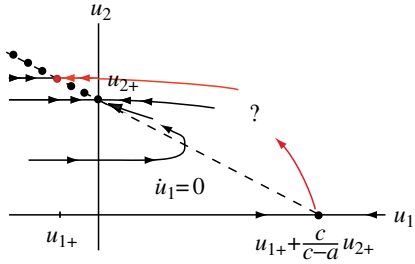

Fig. 12. Phase portrait of (7.2) and (7.3) in P $(u_2 \ge 0)$ for (u_{3+}, c) in Region 1.

unstable manifold of the saddle $(u_{1+} + \frac{c}{c-a}u_{2+}, 0)$ *meets the stable manifold of the degenerate equilibrium* (u_{1+}, u_{2+}).

(2) *Suppose* $u_{2+} < -u_{1+}$. *For* $u_{3*} < u_{3+} < \infty$, *points* (u_{3+}, c) *in Region* 1 *have* $u_{1+} + \frac{c}{c-a}u_{2+} > 0$ (*so the phase portrait of* (7.2) *and* (7.3) *is given by Fig.* 12) *if and only if* $\frac{au_{3+}}{u_{3+}-u_{2+}} < c < \frac{au_{1+}}{u_{1+}+u_{2+}}$. *For each such* u_{3+} *there exists a velocity* c, $\frac{au_{3+}}{u_{3+}-u_{2+}} < c < \frac{au_{1+}}{u_{1+}+u_{2+}}$, *such that the unstable manifold of the saddle* $(u_{1+} + \frac{c}{c-a}u_{2+}, 0)$ *meets the stable manifold of the degenerate equilibrium* (u_{1+}, u_{2+}).

The connections in Proposition 7.2 represent traveling waves of (2.1)–(2.3) of type $FC \xrightarrow{c_f} TC$, with left state $(u_{1-}, u_{2-}, u_{3-}) = (u_{1+} + \frac{c}{c-a}u_{2+}, 0, u_{3+} - \frac{c}{(c-a)}u_{2+})$, and right state (u_{1+}, u_{2+}, u_{3+}). We compute u_{3-} using the fact that w_2 given by (6.13) is constant on solutions. The amount of remaining oxygen, once all the solid fuel has burned is u_{3-}.

Proof of Proposition 7.2. The calculation of the allowed range of c for each $u_{3+} > u_{3*}$ is left to the reader.

Fix $u_{3+} > u_{3*}$.

In case (1), to study the limit $c \to \infty$, divide the right-hand side of (7.2) and (7.3) by c and let $c \to \infty$ (equivalent to a rescaling of time for each c). In the limit we obtain

$$\dot{u}_1 = -(u_1 - u_{1+}) - (u_2 - u_{2+}), \tag{7.9}$$

$$\dot{u}_2 = 0. \tag{7.10}$$

This is the system (7.7) and (7.8) divided by $(a^2u_{2+})^2$. As in the proof of Proposition 7.1, we see that for large c, the stable manifold of (u_{1+}, u_{2+}) lies above the unstable manifold of $(u_{1+} + u_{2+}, 0)$.

In case (2), we substitute $c = \frac{au_{1+}}{u_{1+}+u_{2+}}$ into (7.2) and (7.3) and multiply the right-hand side by $-(u_{1+} + u_{2+}) > 0$, which yields

$$\dot{u}_1 = -au_{2+}(u_1 - u_{1+}) + au_{1+}(u_2 - u_{2+}), \tag{7.11}$$

$$\dot{u}_2 = \frac{1}{a}\left(\frac{u_2 - u_{2+}}{u_{2+}} + \frac{u_{3+}}{au_{1+}}\right) u_2\Phi(u_1). \tag{7.12}$$

The phase portrait is shown in Fig. 13. The stable manifold of (u_{1+}, u_{2+}) lies above the center manifold of the origin, which perturbs to the unstable manifold of $(u_{1+} + \frac{c}{c-a}u_{2+}, 0)$ when c is decreased.

In both cases, using Proposition 7.1, we now see that for $u_{3*} < u_{3+} < \infty$, the configurations of invariant manifolds at large c and on C are opposite. This shows the existence of c. □

7.3. *Region* 2

For (u_{3+}, c) in Region 2, the line $u_3 = 0$ lies between $u_2 = 0$ and $u_2 = u_{2+}$. See Fig. 14, where $(u_2 \geq u_{2+} - \frac{c-a}{c}u_{3+} > 0$, i.e. in $u_3 \geq 0)$, assuming $u_{1+} + u_{3+} > 0$. A traveling wave with right state (u_{1+}, u_{2+}) exists if the unstable manifold of

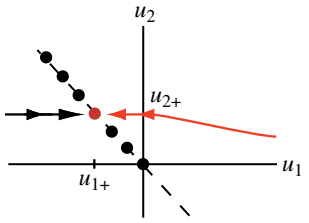

Fig. 13. Phase portrait of (7.11) and (7.12) in P ($u_2 \geq 0$).

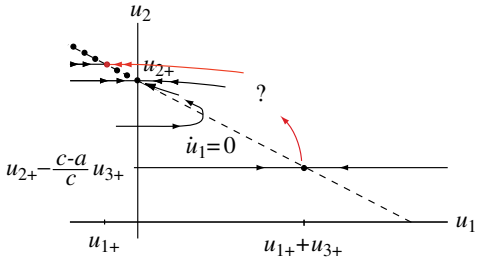

Fig. 14. Phase portrait of (7.2) and (7.3) in P for (u_{3+}, c) in Region 2.

$(u_{1+}+u_{3+}, u_{2+}-\frac{c-a}{c}u_{3+})$ meets the stable manifold of the degenerate equilibrium (u_{1+}, u_{2+}).

Proposition 7.3. *For $a > 0$, $u_{1+} \leq 0$, and $-u_{1+} < u_{3+} < u_{3*}$, u_{3*} given by Proposition* 7.1, *there is a velocity $c > a$ such that the point (u_{3+}, c) lies in Region* 2, *and the stable manifold of (u_{1+}, u_{2+}) contains part of the unstable manifold of $(u_{1+}+u_{3+}, u_{2+}-\frac{c-a}{c}u_{3+})$.*

This connection represents a traveling wave of (2.1)–(2.3) of type $OC \xrightarrow{c_f} TC$, with left state $(u_{1-}, u_{2-}, u_{3-}) = (u_{1+}+u_{3+}, u_{2+}-\frac{c-a}{c}u_{3+}, 0)$, and right state (u_{1+}, u_{2+}, u_{3+}).

Proof of Proposition 7.3. We assume that $u_{2+} > -u_{1+}$; the opposite case is easier. Proposition 7.1(1) gives the relative positions of the stable manifold of (u_{1+}, u_{2+}) and the center manifold of $(u_{1+}+u_{3+}, 0)$ for $(u_{3+}, c) \in C$.

For $-u_{1+} < u_{3+} < u_{2+}$, as $c \to \infty$, the equilibrium $(u_{1+}+u_{3+}, u_{2+}-\frac{c-a}{c}u_{3+})$ approaches $(u_{1+}+u_{3+}, u_{2+}-u_{3+})$. An argument similar to that in the previous section shows that for c very large, the stable manifold of (u_{1+}, u_{2+}) lies above the unstable manifold of $(u_{1+}+u_{3+}, u_{2+}-\frac{c-a}{c}u_{3+})$.

To study the limit $c \to a$ from above for arbitrary u_3, we multiply (7.2) and (7.3) by $c-a$ and set $c=a$. We obtain

$$\dot{u}_1 = 0, \tag{7.13}$$

$$\dot{u}_2 = (u_2 - u_{2+})u_2\Phi(u_1). \tag{7.14}$$

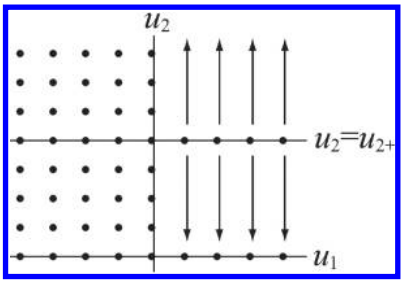

Fig. 15. Phase portrait for (7.13) and (7.14).

The phase portrait is shown Fig. 15. In particular, the half-line of equilibria $u_2 = u_{2+}$, $u_1 > 0$ is normally hyperbolic, and the unstable manifold of a point $(u_{2+}, u_1^\dagger)$ on this half-line is the half-line $u_1 = u_1^\dagger$, $u_2 > 0$. It follows that for c above and close to a, the unstable manifold of $(u_{1+} + u_{3+}, u_{2+} - \frac{c-a}{c}u_{3+})$ is close to a vertical line, and therefore the stable manifold of (u_{1+}, u_{2+}) lies below it.

The conclusion of the proposition follows. □

8. Slow Traveling Waves ($0 < c < a$)

In this section, we shall prove Theorems 3.3 and 3.3.

We assume $0 < c < a$. From Sec. 6, we assume that the right state of a traveling wave of (2.1)–(2.3) is of type OC, i.e. an equilibrium $(u_{1+}, u_{2+}, 0)$ with $u_{1+} > 0$ and $u_{2+} > 0$. Therefore,

$$(w_1, w_2) = ((c-a)u_{1+} + cu_{2+}, -cu_{2+}), \tag{8.1}$$

so the system (6.14) and (6.15) becomes

$$\dot{u}_1 = (a-c)(u_1 - u_{1+}) - c(u_2 - u_{2+}), \tag{8.2}$$

$$\dot{u}_2 = \frac{u_{2+} - u_2}{a-c}u_2\Phi(u_1). \tag{8.3}$$

The invariant line $u_3 = 0$ corresponds to $u_2 = u_{2+}$. P is the region $0 \le u_2 \le u_{2+}$.

Let $u_1^\sharp = u_{1+} - \frac{c}{a-c}u_{2+} < u_{1+}$, $u_2^\dagger = u_{2+} - \frac{a-c}{c}u_{1+} < u_{2+}$. Recall from Sec. 6 the line H defined by $(a-c)u_1 - cu_2 + w_1 = 0$, which contains all equilibria.

Proposition 8.1. *Let $a > 0$, $u_{1+} > 0$, and $u_{2+} > 0$. For each c with $0 < c < a$, one equilibrium of (8.2) and (8.3) is the saddle (u_{1+}, u_{2+}), which corresponds to $(u_1, u_2, u_3) = (u_{1+}, u_{2+}, 0)$. In addition:*

(1) *If $0 < c < \frac{u_{1+}}{u_{1+}+u_{2+}}a$, then $u_1^\sharp > 0$, $u_2^\dagger < 0$, $(u_1^\sharp, 0)$ is a repeller, and there is unique connecting orbit from $(u_1^\sharp, 0)$ to (u_{1+}, u_{2+}), of type FC $\xrightarrow{c_s}$ OC. The line H does not intersect the part of P with $u_1 \le 0$, so the set TC^* is empty. There are no other connecting orbits in P.*

(2) *If* $c = \frac{u_{1+}}{u_{1+}+u_{2+}}a$, *then* $u_1^\sharp = u_2^\dagger = 0$, $(0,0)$ *has one positive and one zero eigenvalue, and there is unique connecting orbit from* $(0,0)$ *to* (u_{1+}, u_{2+}), *of type* $TC \cap FC \xrightarrow{c_s} OC$. *The intersection of the line* H *and* P *is the origin. There are no other connecting orbits in* P.

(3) *If* $\frac{u_{1+}}{u_{1+}+u_{2+}}a < c < a$, *then* $u_1^\sharp < 0$, $u_2^\dagger > 0$, *and* H *meets* P *in the line segment of equilibria*

$$TC^* = \left\{(u_1, u_2) : u_1^\sharp \le u_1 \le 0 \text{ and } u_2 = u_{2+} + \frac{a-c}{c}(u_1 - u_{1+})\right\}.$$

The endpoints of TC^* *are* $(u_1^\sharp, 0)$ *and* $(0, u_2^\dagger)$. *The equilibria in* TC^* *have one* 0 *eigenvalue and one positive eigenvalue.*

In cases (1) *and* (2) *the connecting orbit approaches the right state exponentially; in case* (1), *but not case* (2), *it also approaches the left state exponentially.*

See Fig. 16. The easy proof of this proposition is left to the reader.

Proof of Theorem 3.3(1). The formula for c follows from the equations $w_2 = (c-a)u_{3+} - cu_{2+} = -cu_{2+}$ and $w_2 = (c-a)u_{3-} - cu_{2-} = (c-a)u_{3-}$. The formula for u_{1+} follows from the equations $w_1 = (c-a)u_{1+} + cu_{2+}$ and $w_1 = (c-a)u_{1-} + cu_{2-} = (c-a)u_{1-}$, together with the formula for c. Since $u_{1+} > 0$ and $0 < c < a$, the existence and uniqueness of the wave follow from Proposition 8.1(1) and (2). □

Proof of Theorem 3.3(2). Since w_1 (respectively, w_2) is equal at $(u_1, v_1, u_2, u_3) = (u_{1-}, 0, u_{2-}, u_{3-})$ and $(u_{1+}, 0, u_{2+}, 0)$, we obtain the equations

$$(c-a)u_{1-} + cu_{2-} = (c-a)u_{1+} + cu_{2+}, \quad (c-a)u_{3-} - cu_{2-} = -cu_{2+}.$$

Solving for (u_{2-}, u_{1+}), we obtain

$$u_{2-} = u_{2+} - \frac{a-c}{c}u_{3-}, \quad u_{1+} = u_{1-} + u_{3-}. \tag{8.4}$$

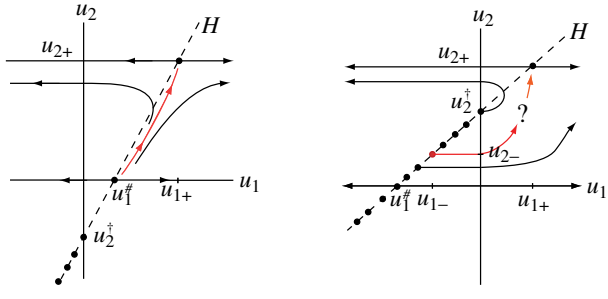

Fig. 16. Phase portrait of (8.2) and (8.3) for $0 < c < a$. (a) $0 < c < \frac{u_{1+}}{u_{1+}+u_{2+}}a$. (b) $\frac{u_{1+}}{u_{1+}+u_{2+}}a < c < a$.

Both are positive as required provided $\frac{u_{3-}}{u_{2+}+u_{3-}}a < c < a$.

Note that $\frac{u_{1+}}{u_{1+}+u_{2+}} < \frac{u_{3-}}{u_{2+}+u_{3-}}$ if and only if $u_{1+} < u_{3-}$, which is true from the formula for u_{1+}. By Proposition 8.1(3), for $\frac{u_{3-}}{u_{2+}+u_{3-}}a < c < a$, the phase portrait is given by Fig. 16(b).

We rewrite (8.2) and (8.3) in terms of the parameters $(u_{1-}, u_{3-}, u_{2+}, c)$ by making the substitutions (8.4), which yields

$$\dot{u}_1 = (a-c)(u_1 - (u_{1-} + u_{3-})) - c(u_2 - u_{2+}), \tag{8.5}$$

$$\dot{u}_2 = \frac{u_{2+} - u_2}{a-c} u_2 \Phi(u_1). \tag{8.6}$$

We consider this system for $\frac{u_{3-}}{u_{2+}+u_{3-}}a < c < a$.

To study the limit $c \to a$ from below, we multiply (8.5) and (8.6) by $a - c > 0$, which yields

$$\dot{u}_1 = (a-c)^2(u_1 - (u_{1-} + u_{3-})) - c(a-c)(u_2 - u_{2+}), \tag{8.7}$$

$$\dot{u}_2 = (u_{2+} - u_2)u_2 \Phi(u_1). \tag{8.8}$$

We then set $c = a$, yielding the system (7.13) and (7.14) multiplied by -1. The flow is given by Fig. 15 with the arrows reversed. The half-lines $u_2 = 0$, $u_1 > 0$ and $u_2 = u_{2+}$, $u_1 > 0$ are respectively normally repelling and normally attracting manifolds of equilibria, with connecting orbits $u_1 =$ constant, $0 < u_2 < 1$. For c close to and less than a, the slow flow on $u_1 > 0$, $u_2 = 0$, which is given by (8.7) with $c = a$, is to the right. From this fact and the signs of $\dot{u}_1$ and $\dot{u}_2$, it follows that for c close to and less than a, the lower branch of the stable manifold of the saddle (u_{1+}, u_{2+}) will, in backward time, rapidly become close to the line $u_2 = 0$ and approach an equilibrium in TC with u_2 close to 0. This will place it below the right branch of the unstable manifold of the point (u_{1-}, u_{2-}) in TC.

To study $c = \frac{u_{3-}}{u_{2+}+u_{3-}}a$, we substitute this value into (8.5) and (8.6), multiply by $u_{2+} + u_{3-} > 0$ and simplify, which yields

$$\dot{u}_1 = au_{2+}(u_1 - u_{1-}) - au_{3-}u_2, \tag{8.9}$$

$$\dot{u}_2 = \frac{1}{au_{2+}}(u_{2+} - u_2)u_2 \Phi(u_1). \tag{8.10}$$

For this system, the point on TC with $u_1 = u_{1-}$ is just $(u_{1-}, 0)$. Its unstable manifold is the u_1-axis, above which is the stable manifold of (u_{1+}, u_{2+}).

From the previous two paragraphs we deduce the existence of the combustion wave for some c in the interval $\frac{u_{3-}}{u_{2+}+u_{3-}}a < c < a$. □

9. Numerical Evidence for Uniqueness

In order to test the uniqueness of the slow combustion waves in Theorem 3.3(2), we rewrite the system (8.2) and (8.3) as one ODE for $u_2(u_1)$:

$$\frac{du_2}{du_1} = \frac{u_{2+} - u_2}{(a-c)^2(u_1 - u_{1+}) - c(a-c)(u_2 - u_{2+})} u_2 \Phi(u_1).$$

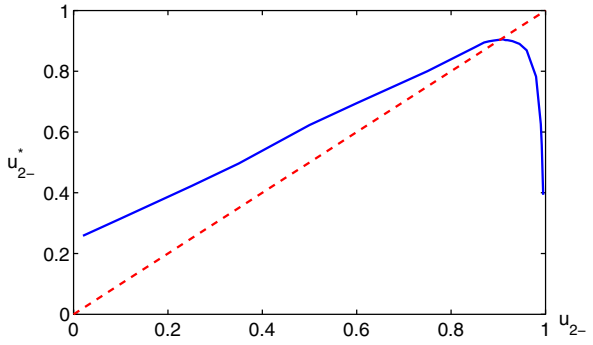

Fig. 17. Map of u_{2-} fixed (horizontal) onto u^*_{2-} resulting from numerical integration (vertical). There is only one fixed point $u_{2-} \approx 0.9$. Values used $u_{1-} = -0.1$, $u_{3-} = 1$, $u_{2+} = 1$ and $a = 5$.

For each set of parameters $\mathcal{P} = (u_{1-}, u_{3-}, u_{2+}, a)$, we could fix u_{2-}, $0 < u_{2-} < u_{2+}$, which determines c and u_{1+} by the formulas in Theorem 3.3(2). We then integrate the ODE from u_{1+} to u_{1-}, assume $u_2(u_{1+}) = u_{2+}$, and obtain a value $u_2 = u^*_{2-}$. A fixed point of the map $u_{2-} \to u^*_{2-}$ gives an orbit that represents a traveling wave.

In order to test numerically the uniqueness of the fixed point, we ran 10,000 simulations for the values of $\mathcal{P}$ in the hypercube $[-0.2, -0.1] \times [1, 2] \times [1, 2] \times [5, 6]$, dividing each side into 10 subintervals to determine grid points.

For each $\mathcal{P}$ we ran about 30 integrations for $u_{2-} \in (0, u_{2+})$. We stopped the integration upon (almost) reaching H or $u_1 = 0$, whichever occurred first. If the integration finished at a point of H with $u_1 > 0$, we took u^*_2 to be the u_2-value of the intersection of H with the u_2 axis. (Backward orbits through points near H with $u_1 > 0$ approach this intersection point very slowly; it would be wasteful to continue the integration further.) The number of fixed points is the number of intersections of the graph of $u_{2-} \to u^*_{2-}$and the line $u^*_{2-} = u_{2-}$. A typical result is plotted in Fig. 17. We found uniqueness for all points tested.

To test the uniqueness of the fast combustion waves in Theorem 3.2 we consider the system (7.2) and (7.3) in an analogous fashion. For each set of parameters $\mathcal{P} = (u_{1+}, u_{2+}, u_{3+}, a)$, we could assume $u_{2-} = 0$ and fix u_{1-}, which determines u_{3-} and c by the formulas in Theorem 3.2. We take $u_{1+} + u_{2+} < u_{1-} < u_{1+} + u_{3+}$; the first inequality ensures $c > a$, the second ensures $u_{3-} > 0$. We then integrate the ODE from u_{1-} to u_{1+}, assume $u_2(u_{1-}) = u_{2-}$, and obtain a value $u_2 = u^*_{2+}$. A fixed point of the map $u_{2-} \to u^*_{2+}$ gives an orbit that represents a traveling wave.

As in the previous case for slow combustion waves, the numerical evidence indicates uniqueness for the fast combustion waves.

Acknowledgments

We thank Fatih Ozbag for finding a mistake in the original version of this paper.

The first two authors were supported in part by: ANP-PRH32 under grant 731948/2010; Petrobras-PRH32 under grant 6000.0069459.11.4; FAPERJ

under grants E-26/102.965/2011, E-26/111.416/2010, E-26/110.658/2012, E-26/111.369/2012, E-26/110.114/2013; CNPq under grants 301564/2009-4, 470635/2012-6, 402299/2012-4; CAPES under grant 17710-12-0; and CAPES/NUFFIC under grant 024/2011. The third author was supported in part by NSF under award DMS-1211707.

Appendix A. Derivation of the Model

We consider one-dimensional flow when air is injected into a porous medium. We use notation and assumptions from [5, 6]. The medium contains initially a fuel that is essentially immobile and does not vaporize. This is the case for solid fuel, or for liquid fuel at low saturations so it does not move. We assume that only a small part of the available space is occupied by the fuel, so that changes of porosity φ during the reaction are negligible. We assume that the solid and gas are at the same temperature (local thermal equilibrium). We also assume that pressure variations are small compared to the prevailing pressure, and we neglect gas expansibility under temperature increase.

The model with time coordinate t and space coordinate x includes the heat balance equation (A.1), as well as the molar balance equations for immobile fuel (A.2) and oxygen (A.3). We assume that the molar density of gas ρ_g [mole/m^3] is constant. (In [1], it depended on temperature.) It follows that the Darcy gas velocity u [m/s] is also constant (equal to the gas injection rate). Gas diffusion is neglected as in [1]. The balance equations for energy, fuel and oxygen are:

$$\frac{\partial((C_m+\varphi c_g\rho_g)(T-T_{\rm res}))}{\partial t}+\frac{\partial(c_g\rho_g u(T-T_{\rm res}))}{\partial x}=\lambda\frac{\partial^2 T}{\partial x^2}+Q_r\rho Y W_r, \quad \text{(A.1)}$$

$$\frac{\partial\rho}{\partial t}=-\mu_f\rho Y W_r, \quad \text{(A.2)}$$

$$\varphi\frac{\partial(Y\rho_g)}{\partial t}+\frac{\partial(Y\rho_g u)}{\partial x}=-\mu_o\rho Y W_r. \quad \text{(A.3)}$$

Here T [K] is the temperature, Y [mole/mole] is the oxygen molar fraction in the gas, ρ [mole/m^3] is the molar concentration of immobile fuel. The remaining quantities are assumed constant as in [1]: C_m [J/m^{3}K], heat capacity of the porous medium; c_g [J/mole K], heat capacity of the gas; $T_{\rm res}$ [K], initial reservoir temperature; λ [J/(m s K)], thermal conductivity of the porous medium; Q_r [J/mole], the immobile fuel combustion enthalpy at $T_{\rm res}$.

We assume that one mole of immobile fuel reacts with one mole of oxygen to generate one mole of gaseous products, as in the reaction $C+O_2\to CO_2$, yielding the scalar stoichiometric coefficients $\mu_f=\mu_o=1$. The reaction rate is usually given by the Arrhenius equation as $W_r=k_p\exp(-E_r/RT)$. Instead we use

$$W_r=\begin{cases}k_p\exp\left(\dfrac{-E}{R(T-T_{\rm ign})}\right), & T>T_{\rm ign},\\ 0, & T\le T_{\rm ign},\end{cases} \quad \text{(A.4)}$$

where E is the activation energy; R is the ideal gas constant; T_{ign} is the temperature below which the reaction is imperceptible; and k_p is the pre-exponential factor.

The equations are nondimensionalized by introducing dimensionless dependent and independent variables (denoted by tildes) as ratios of the dimensional quantities and reference quantities (denoted by stars):

$$\tilde{t} = \frac{t}{t^*}, \quad \tilde{x} = \frac{x}{x^*}, \quad \tilde{\theta} = \frac{T - T_{\text{ign}}}{\Delta T^*}, \quad \tilde{\rho} = \frac{\rho}{\rho^*}, \quad \tilde{Y} = \frac{Y}{Y^*}. \tag{A.5}$$

The reference quantities are chosen to make the equations as simple as possible:

$$\Delta T^* = \frac{E}{R}, \quad t^* = \frac{\varphi Q_r \rho_g}{k_p C_m^* \Delta T^*}, \quad Y^* = \frac{1}{k_p t^*}, \quad \rho^* = \frac{\varphi \rho_g}{k_p t^*}, \quad x^* = \sqrt{\frac{\lambda t^*}{C_m^*}}, \tag{A.6}$$
$$C_m^* = C_m + \varphi c_g \rho_g.$$

Using (A.5) and (A.6) and omitting the tildes, Eqs. (A.1)–(A.4) are written in dimensionless form as follows. The dependent variables are temperature θ ($\theta = 0$ corresponds to $T = T_{\text{ign}}$), oxygen fraction Y and dimensionless fuel concentration ρ:

$$\partial_t \theta + v_\theta \partial_x \theta = \partial_{xx} \theta + \rho Y \Phi, \tag{A.7}$$

$$\partial_t \rho = -\rho Y \Phi, \tag{A.8}$$

$$\partial_t Y + v_Y \partial_x Y = -\rho Y \Phi, \tag{A.9}$$

$$\Phi = \begin{cases} \exp(-1/\theta), & \theta > 0, \\ 0, & \theta \leq 0, \end{cases} \tag{A.10}$$

where v_θ and v_Y are dimensionless thermal and oxygen wave speeds given by:

$$v_\theta = \frac{c_g \rho_g u t^*}{x^* C_m^*}, \quad v_Y = \frac{u t^*}{\varphi x^*}. \tag{A.11}$$

We will need the dimensionless reservoir temperature θ_0 and dimensionless initial fuel concentration ρ_0 given by

$$\theta_0 = \frac{T_{\text{res}} - T_{\text{ign}}}{\Delta T^*}, \quad \rho_0 = \frac{\rho_{\text{res}}}{\rho^*}. \tag{A.12}$$

where ρ_{res} is the initial reservoir molar density of fuel.

A commonly considered limiting case is that the thermal capacity of the gas is negligible compared to the thermal capacity of the substrate, so $C_m^* = C_m + \varphi c_g \rho_g \approx C_m$. Since $v_\theta = (\varphi c_g \rho_g / C_m^*) v_Y$, this implies that $v_\theta \ll v_Y$, which is correct in rock porous media. In this work, we assume instead that the thermal capacity of the substrate is negligible compared to the thermal capacity of the gas, yielding $C_m^* = \varphi c_g \rho_g$ and $v_\theta = v_Y = a$. This assumption is approximately correct for air combustion in polyurethane foam. With these substitutions, system (A.7)–(A.9) becomes the system (2.1)–(2.4).

The reference quantities chosen in (A.6) accomplish the purpose of simplifying the system of partial differential equations. However, when used with realistic data

from [6, 15], they generate nondimensional initial and boundary data that vary over 10 orders of magnitude, making simulation impossible. In the simulations of Sec. 5 we use initial and boundary data of order one with the sole purpose of illustrating the mathematical analysis.

References

[1] I. Y. Akkutlu and Y. C. Yortsos, The dynamics of in-situ combustion fronts in porous media, *J. Combust. Flame* **134** (2003) 229–247.

[2] A. P. Aldushin, I. E. Rumanov and B. J. Matkowsky, Maximal energy accumulation in a superadiabatic filtration combustion wave, *J. Combust. Flame* **118** (1999) 76–90.

[3] A. P. Aldushin and B. S. Seplyarsky, Propagation of exothermic reaction in a porous-medium during gas blowing, *Sov. Phys. Dokl.* **23** (1978) 483–485.

[4] J. Bruining, A. A. Mailybaev and D. Marchesin, Filtration combustion in wet porous medium, *SIAM J. Appl. Math.* **70** (2009) 1157–1177.

[5] G. Chapiro, Gas-solid combustion in insulated porous media, Doctoral thesis, IMPA (2009), http://www.preprint.impa.br.

[6] G. Chapiro, A. A. Mailybaev, A. J. Souza, D. Marchesin and J. Bruining, Asymptotic approximation of long-time solution for low-temperature filtration combustion, *Comput. Geosci.* **16** (2012) 799–808.

[7] J. C. Da Mota and M. M. Santos, An application of the monotone iterative method to a combustion problem in porous media, *Nonlinear Anal. Real World Appl.* **12**(2) (2011) 1192–1201.

[8] A. Ghazaryan, Y. Latushkin and S. Schecter, Stability of traveling waves for a class of reaction–diffusion systems that arise in chemical reaction models, *SIAM J. Math. Anal.* **42**(6) (2010) 2434–2472.

[9] A. Ghazaryan, Y. Latushkin, S. Schecter and A. J. de Souza, Stability of gasless combustion fronts in one-dimensional solids, *Arch. Ration. Mech. Analy.* **198**(3) (2010) 981–1030.

[10] C. K. R. T. Jones, *Geometric Singular Perturbation Theory*, in *Dynamical Systems*, Lecture Notes in Mathematics, Vol. 1609 (Springer, Berlin, 1995), pp. 44–118.

[11] A. A. Mailybaev, J. Bruining and D. Marchesin, Analysis of in situ combustion of oil with pyrolysis and vaporization, *Combust. Flame* **158**(6) (2011) 1097–1108.

[12] A. A. Mailybaev, D. Marchesin and J. Bruining, Resonance in low-temperature oxidation waves for porous media, *SIAM J. Math. Anal.* **43** (2011) 2230–2252.

[13] D. Marchesin and S. Schecter, Oxidation heat pulses in two-phase expansive flow in porous media, *Z. Angew. Math. Phys.* **54**(1) (2003) 48–83.

[14] J. C. D. Mota and S. Schecter, Combustion fronts in a porous medium with two layers, *J. Dynam. Differential Equations* **18**(3) (2006) 615–665.

[15] K. Prasad, R. Kramer, N. Marsh, M. Nyden, T. Ohlemiller and M. Zammarano, Numerical simulation of fire spread on polyurethane foam slabs, in *Proc. 11th Int. Conf. Fire and Materials* (Interscience Communications, London, 2009), pp. 697–708.

[16] S. Schecter, The saddle-node separatrix-loop bifurcation, *SIAM J. Math. Anal.* **18**(4) (1987) 1142–1156.

[17] S. Schecter and D. Marchesin, Geometric singular perturbation analysis of oxidation heat pulses for two-phase flow in porous media. *Bull. Braz. Math. Soc.* **32**(3) (2001) 237–270. Dedicated to Constantine Dafermos on his 60th birthday.

[18] D. A. Schult, B. J. Matkowsky, V. A. Volpert and A. C. Fernandez-Pello, Forced forward smolder combustion, *Combust. Flame* **104**(1–2) (1996) 1–26.

[19] C. Wahle, B. Matkowsky and A. Aldushin, Effects of gas-solid nonequilibrium in filtration combustion, *Combust. Sci. Technol.* **175** (2003) 1389–1499.
[20] Y. B. Zeldovich, G. I. Barenblatt, V. B. Librovich and G. M. Makhviladze, *The Mathematical Theory of Combustion and Explosion* (Consultants Bureau, New York, 1985).